



Article

Design and Synthesis of Novel Reactive Oxygen Species Inducers for the Treatment of Pancreatic Ductal Adenocarcinoma

Yuting Kuang, Mario Sechi, Salvatore Nurra, Mats Ljungman, and Nouri Neamati

J. Med. Chem., **Just Accepted Manuscript** • DOI: 10.1021/acs.jmedchem.7b01463 • Publication Date (Web): 12 Jan 2018

Downloaded from <http://pubs.acs.org> on January 12, 2018

Just Accepted

“Just Accepted” manuscripts have been peer-reviewed and accepted for publication. They are posted online prior to technical editing, formatting for publication and author proofing. The American Chemical Society provides “Just Accepted” as a free service to the research community to expedite the dissemination of scientific material as soon as possible after acceptance. “Just Accepted” manuscripts appear in full in PDF format accompanied by an HTML abstract. “Just Accepted” manuscripts have been fully peer reviewed, but should not be considered the official version of record. They are accessible to all readers and citable by the Digital Object Identifier (DOI®). “Just Accepted” is an optional service offered to authors. Therefore, the “Just Accepted” Web site may not include all articles that will be published in the journal. After a manuscript is technically edited and formatted, it will be removed from the “Just Accepted” Web site and published as an ASAP article. Note that technical editing may introduce minor changes to the manuscript text and/or graphics which could affect content, and all legal disclaimers and ethical guidelines that apply to the journal pertain. ACS cannot be held responsible for errors or consequences arising from the use of information contained in these “Just Accepted” manuscripts.



(*Journal of Medicinal Chemistry*)

Design and Synthesis of Novel Reactive Oxygen Species Inducers for the Treatment of Pancreatic Ductal Adenocarcinoma

Yuting Kuang,^{†,§} Mario Sechi,^{¶,*} Salvatore Nurra,[¶] Mats Ljungman,[£] and Nouri Neamati^{†,*}

[†]Department of Medicinal Chemistry, College of Pharmacy, University of Michigan, 1600 Huron Parkway, Ann Arbor, MI 48109, United States

[§]Department of Pharmacology and Pharmaceutical Sciences, School of Pharmacy, University of Southern California, 1985 Zonal Avenue, Los Angeles, CA 90033, United States

[¶]Department of Chemistry and Pharmacy, University of Sassari, Via Vienna 2, 07100 Sassari, Italy

[£]Department of Radiation Oncology, University of Michigan, 1600 Huron Parkway, Ann Arbor, MI 48109, United States

1
2
3 **ABSTRACT:** Altering redox homeostasis provides distinctive therapeutic opportunities for
4
5 the treatment of pancreatic cancer. Quinazolinediones (QDs) are novel redox modulators that we
6
7 previously showed to induce potent growth inhibition in pancreatic ductal adenocarcinoma
8
9 (PDAC) cell lines. Our lead optimization campaign yielded QD325 as the most potent redox
10
11 modulator candidate inducing substantial reactive oxygen species (ROS) in PDAC cells. Nascent
12
13 RNA sequencing following treatments with the QD compounds revealed induction of stress
14
15 responses in nucleus, endoplasmic reticulum, and mitochondria of pancreatic cancer cells.
16
17 Furthermore, the QD compounds induced Nrf2-mediated oxidative stress and unfolded protein
18
19 responses as demonstrated by dose dependent increases in RNA synthesis of representative genes
20
21 such as *NQO1*, *HMOX1*, *DDIT3* and *HSPA5*. At higher concentrations, the QDs blocked
22
23 mitochondrial function by inhibiting mtDNA transcription and downregulating the mtDNA-
24
25 encoded OXPHOS enzymes. Importantly, treatments with QD325 were well tolerated *in vivo* and
26
27 significantly delayed tumor growth in mice. Our study supports the development of QD325 as a
28
29 new therapeutic in the treatment of PDAC.
30
31
32
33
34
35
36
37

38 **Keywords:** Pancreatic Cancer, ROS, Next-generation Sequencing, Unfolded Protein Response,
39
40 Mitochondrial Synthesis
41
42
43
44
45
46
47
48
49
50
51
52
53
54
55
56
57
58
59
60

INTRODUCTION

Pancreatic cancer is the fourth leading cause of cancer-related death in both genders in the United States, estimated to claim over 40,000 lives in 2017.¹ Given its asymptomatic and metastatic nature, over 50% of pancreatic cancer cases are diagnosed at late stages, when the tumor has metastasized and is often unresectable.² Therefore, treatment of pancreatic cancer is largely dependent on systemic chemotherapy. Ever since its approval by the FDA in 1996, gemcitabine-based regimens have been the standard of care for pancreatic cancer.³ However, limited by late-stage diagnosis and inherent/acquired resistance to available chemotherapy, the overall five-year survival rate of pancreatic cancer is only 6.7%, one of the lowest among all types of cancers. Recently, two combination regimens with modest clinical activity have been added as an option for pancreatic cancer patients. The combination of nab-paclitaxel (albumin-bound paclitaxel) with gemcitabine has increased median overall survival from 6.7 to 8.5 months.⁴ The combination cocktail including oxaliplatin, irinotecan, fluorouracil and leucovorin (FOLFIRINOX) was approved for the treatment of metastatic pancreatic cancer by improving median overall survival from 6.8 months in the gemcitabine group to 11.1 months in the FOLFIRINOX group,⁵ but increased toxicity is the major concern for these new treatment options.⁶⁻⁸ Therefore, novel therapeutics are urgently needed to enhance the survival and quality of life of patients with this devastating disease.⁹⁻¹¹

Modulation of redox homeostasis in cancer cells provides a new opportunity for tumor intervention.¹²⁻¹⁸ Reactive oxygen species (ROS), natural byproducts from mitochondrial respiration and other cellular processes, play important roles as second messengers in cell signaling.¹⁹ However, when present at high concentrations, ROS can be detrimental to cells by inducing oxidative damage to DNA, lipids and proteins.²⁰ Cells eliminate excess intracellular

1
2
3 ROS via expression of antioxidant genes regulated by the ROS-detoxifying machinery. In tumor
4 cells, antioxidant enzymes are often induced as a result of elevated levels of intrinsic ROS.²¹
5
6 Expression of mutant oncogenic Kras^{G12D}, commonly present in pancreatic ductal
7 adenocarcinoma (PDAC), keeps the master transcription factor NRF2 elevated at basal state to
8 mount an antioxidant response.²²⁻²⁵ A shift in the redox homeostasis is expected to make tumor
9 cells more susceptible to induced oxidative stress, overwhelming their adaptive antioxidant
10 capacity and promoting ROS-mediated cell death.²⁶⁻²⁸
11
12
13
14
15
16
17
18

19 Among various classes of small-molecule drugs tested in our laboratory to induce ROS,
20 the quinone containing compounds showed great promise due to their significant increase in
21 oxygen consumption rate in treated cells. Many quinones inhibit multiple biochemical assays due
22 to their redox, metal-chelation, color, and in some cases, reactivity towards nucleophiles through
23 Michael addition. Therefore, they are classified as pan assay inhibitors in high throughput
24 screening campaigns. However, over two-dozen drugs containing a quinone moiety have been
25 approved by the FDA or are under clinical investigations not only in oncology but also in other
26 diseases. For example, doxorubicin and dozen of its analogs, mitoxantrone, and mitomycin C are
27 some of the most commonly used FDA approved chemotherapeutic agents for numerous cancers
28 that contain a quinone group. In addition, there are many other agents that are approved for
29 various indications or are in late stage clinical development that broadly fall under the quinone
30 class of drugs (Chart 1).
31
32
33
34
35
36
37
38
39
40
41
42
43
44
45

46 Previously, we showed that the quinazolinone QD232 (Chart 2) exerts ROS-mediated
47 cytotoxicity in pancreatic cancer models.^{29, 30} In this study, we performed a lead optimization
48 campaign and identified QD325 as a lead compound for in-depth preclinical and mechanistic
49
50
51
52
53
54
55
56
57
58
59
60

1
2
3 studies. Several major modifications on QD232 were made by varying the substituents at the
4
5 nitrogen atom on position 6 of the quinazoline-5,8-dione backbone.
6

7
8 Specifically, mono/poly substitution on the phenyl ring with various functionalities
9
10 and/or bulky aromatic system was mainly explored to modulate lipophilicity and steric effects
11
12 (Chart 2). Furthermore, to evaluate a potential synergistic effect in terms of ROS modulation, we
13
14 sought to conjugate the quinazoline-5,8-dione scaffold to a highly lipophilic
15
16 triphenylphosphonium cation for mitochondrial targeting.^{31, 32} Disruption of mitochondrial-
17
18 mediated cell redox modulation represents a promising avenue for future therapy in cancer. Since
19
20 our compounds increase ROS production we tested their ability to interfere with mitochondrial
21
22 processes.
23
24
25

26
27 Our results show that QD325 caused selective inhibition of transcription of the
28
29 mitochondrial genome potentially by abrogating the mitochondrial D-loop, critical for mt-DNA
30
31 transcription. We propose that such targeting could be efficacious and should be further
32
33 explored as an innovative therapeutic approach to target cancers that heavily depend on
34
35 mitochondrial function. Importantly, QD325 was found to be well tolerated and showed tumor-
36
37 suppressing activities in a pancreatic cancer xenograft model.
38
39
40
41
42
43
44
45
46
47
48
49
50
51
52
53
54
55
56
57
58
59
60

RESULTS

Chemistry. The synthesis of compounds QD324-338, 353-357 (Table 1) was carried out using Bracher's methodology, according to our previously reported procedure with some modifications. Scheme 1 illustrates the synthesis of the key synthon QD323 from the readily available dimethoxybenzaldehyde (**1**). Nitration of compound **1** with concentrated nitric acid in the presence of acetic anhydride under simple magnetic stirring afforded the 3,6-dimethoxy-2-nitrobenzaldehyde (**2**) in good yield. This regioisomer was converted to the diformamido-derivative **3** under gaseous HCl. Compound **3** was then cyclized to dimethoxyquinazoline **4** by treatment with zinc powder and acetic acid. Final oxidation by cerium ammonium nitrate resulted in the production of quinazoline-5,8-dione QD323. Regioselective addition of appropriate aminobenzenes to 6 position of QD323 in the presence of Ce(III) ions gave QD324-338, 353-357 (Schemes 2 and 3).

Then, we wanted to obtain triphenylphosphonium-based model derivatives of compound QD331 and QD232. Compounds QD340 and QD359 were therefore generated by adapting a phosphine conjugation method, as we previously described.³¹⁻³³ The synthesis of triphenylphosphonium-based compounds QD340 and QD359 is illustrated in Schemes 4 and 5. Initially, 3-bromopropylamine hydrobromide (**5**) was reacted with triphenylphosphine in refluxing acetonitrile for 16 hours, and the resulting triphenylphosphonium intermediate (**6**) was isolated after treatment with n-hexane/diethyl ether/isopropanol. Next, the 4- and 3-aminobenzamido-propyl-triphenylphosphonium bromides QD339 and QD358 were prepared by conjugating **6** with 4- or 3-aminobenzoic acid, respectively, via a standard coupling protocol using DIPEA, HBTU, DMAP, in CH₂Cl₂. Finally, QD340 and QD359 were obtained by nucleophilic addition of

1
2
3 appropriate triphenylphosphonium salts (QD339 or QD358) to QD323 in the presence of Ce(III),
4
5 according to the above-mentioned procedure.
6
7
8
9

10 **QD Compounds Inhibit Proliferation of Pancreatic Cancer Cells.** We designed and
11 synthesized 25 new analogues of our previous lead compound, QD232, to better elucidate their
12 mechanisms of action. Nine of these novel analogues showed improved cytotoxicity compared to
13 QD232 in at least two PDAC cell lines in MTT assay (Table 1). QD325 was found to be the most
14 potent analogue with IC₅₀ values <1 μM in the three PDAC cell lines (MIA PaCa-2, Panc-1, and
15 BxPC-3).
16
17
18
19
20
21
22

23 QD325 (as well as QD232) showed similar dose-dependent cytotoxicity in MIA PaCa-2
24 and a gemcitabine-resistant derivative cell line MIA PaCa-2-GR³⁴ (Table 2). In HPV16-E6E7
25 immortalized pancreatic cell line HPDE,³⁵ gemcitabine produced similar IC₅₀ values as MIA
26 PaCa-2 cells, while the most potent QD325 compound showed a 3-fold higher sensitivity for
27 MIA PaCa-2 (Table 2).
28
29
30
31
32
33
34
35
36

37 **Cytotoxicity of QD Compounds Correlates with Increased ROS Production.**

38 Treatment with the QD compounds elicited significant ROS accumulation in MIA PaCa-2 cells
39 as shown in the H2DCFDA reactivity assay (Figures 1 and S2). To validate ROS induction as the
40 mechanism for cytotoxicity, the effect of QD compounds were evaluated in the presence and
41 absence of the antioxidant N-acetyl-cysteine (NAC). For the lead compound QD232 and the two
42 active analogues QD325 and QD326, we observed a time- and dose-dependent accumulation of
43 ROS (Figure 1A). While H₂O₂ treatment lead to an immediate conversion of H2DCFDA to
44 fluorescent DCF, treatment with the QD compounds resulted in a gradual induction of the
45
46
47
48
49
50
51
52
53
54
55
56
57
58
59
60

1
2
3 fluorescent signal, which reached peak levels after 4-6 h, implying a progressive ROS
4
5 accumulation.
6

7
8 When cells were pretreated with 5 mM NAC, ROS induction by H₂O₂ and the QD
9
10 compounds was blocked (Figure 1B). In the MTT cell proliferation assay, NAC attenuated the
11
12 proliferation inhibitory effect of H₂O₂, QD232, QD325 and QD326 (Figure 1C). Importantly, we
13
14 did not observe any colloidal behavior or aggregation for QD compounds in our assays. These
15
16 results demonstrate that ROS accumulation is a major mechanism for cytotoxicity of the QD
17
18 compounds. However, NAC treatment did not completely block the effect of the QD compounds
19
20 and H₂O₂, suggesting these compounds may induce additional cellular effects responsible for the
21
22 inhibition of cell proliferation. Testing many analogues in the presence of NAC and GSH at 1 to
23
24 5 mM we discovered that these antioxidants could protect toxicity anywhere from 10-80%
25
26 depending on the analogue. In most cases NAC addition never fully protects the cells even at
27
28 1000-fold excess of antioxidant. These studies suggest that the compounds not only produce
29
30 ROS but also bind to unique targets. It is also possible that the QD-NAC conjugate is partially
31
32 responsible for the ROS induction and cytotoxicity.
33
34
35
36
37

38 The faster induction of oxidative stress by the optimized compounds is perhaps due to
39
40 improved membrane permeability (predicted cLogP values for QD232 and QD325 are 1.99 and
41
42 3.89, respectively). We expected that better *in vitro* antiproliferative activity of QD325 should
43
44 translate to better *in vivo* efficacy. Therefore, we selected QD325 for extensive mechanistic and
45
46 *in vivo* studies.
47
48
49
50

51 In order to selectively target these compounds to the mitochondria, we synthesized two
52
53 derivatives containing a triphenylphosphine group. To our surprise, QD340 and QD359 did not
54
55
56
57
58
59
60

1
2
3 show better ROS induction and cytotoxicity than QD325 and were not further explored. A
4 possible explanation of this unexpected behavior could be attributed to their redox properties,
5 since we previously showed that triphenylphosphoniums decreased cellular oxygen consumption
6 rate (OCR). Furthermore, the QD compounds without the triphenylphosphonium group cause a
7 remarkable increase in cellular OCR.³⁰
8
9
10
11
12
13
14
15
16

17 **The QD Compounds Induce Oxidative Stress and the Unfolded Protein Response.**

18
19 We used the recently established bromouridine labeled RNA sequencing (Bru-seq) technique to
20 better characterize transcriptional effects of the QD compounds. Bru-seq captures nascent RNA
21 and provides information on ongoing transcription genome-wide without interference by pre-
22 existing RNA.^{36, 37} We observed that the transcription signatures induced by 4-hour treatments
23 with QD232 or QD325 were similar according to Ingenuity Pathway Analysis (IPA) or Gene Set
24 Enrichment Analysis (GSEA) of the expressed genes (Figures 2 and S3-S6). This implies that the
25 two compounds have similar mechanisms of action. IPA profiling of all genes with >1.5-fold
26 change in expression upon treatment of MIA PaCa-2 cells with QD232 or QD325 identified the
27 “NRF2-mediated oxidative stress response” and “unfolded protein response” (UPR) as key
28 pathways activated by these compounds (Figure 2A).
29
30
31
32
33
34
35
36
37
38
39
40
41

42 NRF2 is a transcription factor that is rapidly activated in response to oxidative and
43 electrophilic exposure and it promotes the transcription of genes encoding various detoxifying
44 enzymes.³⁸ Upon oxidative challenge, KEAP1 inactivation allows nascent NRF2 proteins to
45 translocate to the nucleus,^{39, 40} and activate transcription of antioxidant genes containing AREs
46 (antioxidant response element) or MAREs (MAF recognition element) in *cis*-acting enhancer
47 elements.
48
49
50
51
52
53
54
55
56
57
58
59
60

1
2
3 *NQO1* and *HMOX1* are two target genes of NRF2 that counteract the effects of oxidative
4 stress.^{41,42} *NQO1* encodes the flavoprotein NAD(P)H:quinone oxidoreductase 1 that catalyzes a
5 two-electron reduction of quinones to hydroquinones and exhibits chemo-protective effects.^{43,44}
6
7
8
9
10 *HMOX1* encodes heme oxygenase 1 (HO-1), whose antioxidant properties arise from
11 degradation of the pro-oxidant heme and production of antioxidant bilirubin from biliverdin.⁴⁵
12
13 As revealed by Bru-seq, synthesis of *NQO1* and *HMOX1* RNAs was upregulated in a dose-
14 dependent manner by treatments with either QD232 or QD325 (Figure 2B).
15
16
17
18

19 The unfolded protein response (UPR) comprises three pathways regulated by the ER
20 trans-membrane proteins inositol-requiring enzyme 1a (IRE1a), activating transcription factor 6
21 (ATF6), and protein kinase RNA-like endoplasmic reticulum kinase (PERK), respectively.⁴⁶⁻⁴⁸
22
23 Misfolded proteins in the ER lumen trigger the competitive binding of the ER chaperone GRP78,
24 leading to the activation of IRE1a, ATF6 and PERK and downstream responses to UPR.⁴⁹
25
26 Depending on the severity and duration of the ER stress, the UPR can function as a pro-survival
27 mechanism and restore homeostasis, or trigger apoptosis if the stress burden is beyond the
28 capacity of this adaptive response.^{50,51}
29
30
31
32
33
34
35
36

37 *DDIT3* and *HSPA5* are genes that are induced as a result of UPR signaling. *HSPA5*
38 encodes GRP78, the key regulatory protein of ER stress. *DDIT3* is a downstream target gene that
39 transcriptionally responds to all three arms of the UPR. As a transcription factor, the *DDIT3* gene
40 product CHOP promotes apoptosis under prolonged ER stress by inducing transcription of pro-
41 apoptotic genes including PUMA and BIM.⁵²⁻⁵⁴ Transcription of the two stress responsive genes
42
43
44
45
46
47
48
49 *DDIT3* and *HSPA5* is significantly increased by QD232 or QD325 treatment in a dose-dependent
50 manner (Figure 2C).
51
52
53
54
55
56
57
58
59
60

1
2
3 Upregulation of mRNA synthesis detected by Bru-seq was found to also result in
4 increased protein levels of the major stress responsive genes. We observed time-dependent
5 increased protein levels of CHOP and GRP78 in MIA PaCa-2, Panc-1, and BxPC-3 cells treated
6 with the QD compounds (Figure 3A-C). For the oxidative stress responsive genes, *HO-1* was
7 upregulated by QD treatments in MIA PaCa-2 and BxPC-3 cells, while no significant change
8 was detected in Panc-1 cells. Of note, the *NQO1* gene is known to be deleted in Panc-1 cells, and
9 as expected, no transcription of the gene was observed in this cell line using Bru-seq. In MIA
10 PaCa-2 and BxPC-3, *NQO1* showed high basal expression levels with no further induction
11 following treatment. These results suggest that MIA PaCa-2 and BxPC-3 cells have a high
12 intrinsic oxidative stress burden and that this may make them sensitive to exogenous agents
13 inducing oxidative stress. Indeed, IPA analysis showed significant activation of apoptosis
14 signaling at higher concentration of QD232 (3 times IC_{50}) or QD325 (5 times IC_{50}) after 4 h
15 treatment (Figure S3), suggesting that apoptosis is a mode of death following exposure to the QD
16 compounds.
17
18

19
20
21 Previously, it was shown that ROS-inducing compounds such as phenethylisothiocyanate
22 and curcumin efficiently downregulate specificity protein (Sp) transcription factors Sp1, Sp3,
23 and Sp4 in pancreatic cancer cells,⁵⁵⁻⁵⁷ however, we did not observe selective downregulation of
24 these transcription factor genes in our Bru-seq studies and these factors were not in our top 100
25 affected genes.
26
27

28
29
30 **The QD Compounds Inhibit Transcription of mtDNA from the D-loop.** Mitochondria
31 play an important role in regulating redox homeostasis in mammalian cells. Deregulation of the
32 expression of mitochondrial genes can lead to interruption of the oxidative phosphorylation
33 pathway, resulting in the accumulation of ROS. Mitochondrial DNA (mtDNA) harbors 13 genes
34
35
36
37
38
39
40
41
42
43
44
45
46
47
48
49
50
51
52
53
54
55
56
57
58
59
60

1
2
3 that encode proteins with important functions in the electron transport chain. The double-
4
5 stranded circular mitochondrial genome comprises the guanine-rich heavy strand and the
6
7 cytidine-rich light strand. Using Bru-seq, we observed significant inhibition of mtDNA
8
9 transcription after a 4-hour treatment with QD compounds at higher concentrations (Figure 4A;
10
11 Figure S7). Both compounds decreased COX III protein levels, which correlated to a reduced
12
13 rate of transcription of the gene (Figure 4B). These results strongly suggest that the QD
14
15 compounds disrupt mitochondrial function.
16
17
18

19 The D-loop (displacement loop) is a noncoding area of the mtDNA genome composed of
20
21 a short three-stranded structure required for the regulation of initiation of mtDNA replication and
22
23 transcription. This region contains two promoters on the heavy strand HSP1 and HSP2, one on
24
25 the light strand, LSP, and also the mtDNA replication origin O_H . The D-loop region has been
26
27 reported to be frequently mutated in lung, hepatocellular, colorectal and cervical cancers⁵⁸⁻⁶¹ and
28
29 these D-loop mutations are linked to a poor prognosis of the disease.^{62, 63}
30
31
32

33 Using Bru-seq we found that the QD compounds inhibited the transcription of mtDNA
34
35 from both the heavy strand promoter HSP2 (top long arrow in Figure 4A) and the light strand
36
37 promoter LSP (bottom arrow), thus inhibiting the expression of mitochondrial genes that are
38
39 essential for mitochondrial oxidative phosphorylation. However, the activity of the heavy strand
40
41 promoter HSP1 (top short arrow, Figure 4A), which regulates transcription of 12s rRNA and 16s
42
43 rRNA, was less affected by the QDs. This pattern of transcriptional inhibition was not observed
44
45 following treatments with UV light, camptothecin or with 40 FDA approved and other novel
46
47 drugs developed in our laboratory (data not shown). Thus, the Bru-seq data showing selective
48
49 transcriptional inhibition of the mitochondrial genome suggest that this mechanism may be
50
51 linked to the toxicity induced by the QD232 and QD325 compounds.
52
53
54
55
56
57
58
59
60

1
2
3
4
5
6 **QD325 Delays Tumor Growth without Systemic Toxicity.** In NOD/SCID mice, MIA
7
8 PaCa-2-derived xenograft showed significantly delayed growth following treatment with QD325
9
10 (5 mg/kg). On day 44 the xenografts treated with QD325 had only reached a size of 308 ± 72
11
12 mm^3 ($p = 2.1\text{E}6$) compared to $1291 \pm 168 \text{mm}^3$ for the xenografts in the control group (Figure
13
14 5A).
15

16
17 No symptoms of gross toxicity such as weakness, weight loss or lethargy were observed
18
19 in any treatment group for the duration of the treatments (Figure 5B). H&E stained organ
20
21 sections did not reveal any major histopathological changes, further confirming the *in vivo*
22
23 tolerability of QD325 (Figure 5C). Following the 44-day treatment, two mice from each group
24
25 were used to evaluate efficacy and safety of QD325 at higher doses. While tumors in the control
26
27 group exhibited rapid growth, QD325 treatment was able to delay growth of the tumors without
28
29 any overt systemic toxicity observed even at doses as high as 20 mg/kg (Figure 6A-B).
30
31

32
33 In line with the tumor growth inhibition, QD325 treatment decreased the staining for the
34
35 proliferation marker Ki67 in tumor tissues, suggesting inhibition of cell proliferation (Figure 5D).
36
37 To further evaluate the mechanisms of action of QD325 *in vivo*, we examined the protein levels
38
39 of stress response markers in tumor lysates. NQO1, HO-1, CHOP and GRP78 protein levels
40
41 were significantly upregulated in QD325 treated tumors compared to tumors treated with vehicle,
42
43 further confirming induction of oxidative stress and UPR as major mechanisms of action for
44
45 QD325 in these pancreatic cancer models (Figure 5E).
46
47
48

49 Gemcitabine is currently used as the standard of care for treatment of pancreatic cancer
50
51 patients. Unfortunately, inherent or acquired resistance to gemcitabine represents a major
52
53 challenge for successful treatment of this disease. Here we sought to explore the potential
54
55
56
57
58
59
60

1
2
3 efficacy of administering QD325 in combination with gemcitabine. In mice studies, gemcitabine
4 is usually given at high doses (40-160 mg/kg) twice weekly. Considering its low tolerance in
5 NOD/SCID mice, we compared antitumor activity of two different gemcitabine treatment
6 schedules in a MIA PaCa-2 xenograft model in this mouse strain: 1) 15 mg/kg once a week for
7 48 days; 2) 15 mg/kg twice a week for the first 15 days. Similar antitumor activity was achieved
8 by either schedule (Figure 6C). In both cases, gemcitabine was well tolerated and no weight loss
9 was observed (Figure 6D). Therefore, schedule 1 was used for comparison of efficacy with
10 QD325 at 5 mg/kg and the combination of gemcitabine and QD325. QD325 was given at 5
11 mg/kg five times a week and gemcitabine was given at 15 mg/kg once a week (Figure 6E). At
12 the end of the 48-day treatment period, average tumor size was $1503 \pm 189 \text{ mm}^3$ for the control
13 group, $387 \pm 74 \text{ mm}^3$ ($p = 0.0049$) for the gemcitabine group, $248 \pm 72 \text{ mm}^3$ ($p = 0.0030$) for
14 the QD325 group, and $163 \pm 83 \text{ mm}^3$ ($p = 0.0023$) for the combination of gemcitabine and
15 QD325 group (Figure 6E). Single agent treatment with QD325 at 5 mg/kg showed similar anti-
16 tumor activity as gemcitabine. In this experiment, both gemcitabine and QD325 greatly inhibited
17 tumor growth as single agents. Importantly, the combination was well tolerated and no weight
18 loss was observed in any of the treatment groups, suggesting a reasonable safety profile of the
19 drug combination (Figure 6F).
20
21
22
23
24
25
26
27
28
29
30
31
32
33
34
35
36
37
38
39
40
41
42
43

44 DISCUSSION

45
46
47 Altered redox homeostasis has been observed in various types of cancers including
48 PDAC. ROS levels are increased as a result of elevated energy demands in cancer cells. To adapt
49 to changes in the microenvironment, cancer cells hijack the intracellular antioxidant machinery
50 to reach a new redox state that can facilitate their proliferation. Such dependency on an altered
51
52
53
54
55
56
57
58
59
60

1
2
3 redox state provides novel therapeutic opportunities. Previously, we provided proof of concept
4 that generation of additional ROS using the tool compound QD232 can lead to the selective
5 killing of cancer cells when they are challenged beyond their antioxidant capacity.^{29, 30} In order
6 to expand upon our previous observations and to select a compound for future clinical
7 development, we performed a lead optimization campaign and identified QD325, which showed
8 a stronger induction of ROS and more potent cytotoxicity in PDAC cells (Figure 1).
9
10
11
12
13
14
15
16

17 As revealed by nascent RNA Bru-seq analysis, the NRF2-mediated oxidative stress
18 response is induced within 4 hours of treatment with the QD compounds (Figure 2). The
19 cytoprotective NRF2 signaling pathway has been found to be cancer preventive under certain
20 circumstances but oncogenic under other conditions.^{64, 65} Activating mutations in NRF2 and
21 KEAP1 are often seen in cancers as an adaptation to elevated intrinsic ROS levels.⁶⁶ In PDAC,
22 where such mutations are not very common, the redox state alteration can be supported through
23 other pathways. The Kras^{G12D} mutation found in >90% of PDAC cases, activates the Nrf2
24 signaling through the MAPK pathway, thus modifying the antioxidant program of PDAC cells to
25 promote tumor progression.²² This subtle balance is crucial for cancer cells as knockdown of
26 NRF2 in PDAC cell lines results in decreased cell viability,⁶⁷ showing dependency of cell
27 proliferation on the antioxidant pathway.
28
29
30
31
32
33
34
35
36
37
38
39
40
41

42 The NRF2 inhibitor, trig, can significantly sensitize PDAC cells to etoposide or TRAIL-
43 induced apoptosis, and also enhances the antitumor response to etoposide in xenograft models.⁶⁸
44 However, trig was not cytotoxic as a single agent and the sensitization of cells was dependent on
45 the proteasome degradation pathway. An alternative strategy to target the altered redox balance
46 in cancer cells would be to trigger ROS accumulation. ROS inducing-agents such as QD232,³⁰
47 piperlongumine,⁶⁹ and imexon⁷⁰ have shown single agent anti-tumor activities in pancreatic
48
49
50
51
52
53
54
55
56
57
58
59
60

1
2
3 cancer models. Induction of ROS by the QD compounds alters this delicate balance and cells
4
5 respond by upregulating the NRF2 pathway in an effort to counter the insult. However, excessive
6
7 ROS overwhelms the system to the point of no return leading to cell death. A phase I trial of
8
9 imexon and gemcitabine in patients with advanced pancreatic cancer demonstrated feasibility
10
11 and antitumor responses⁷¹ encouraging clinical testing of more potent compounds such as
12
13 QD325. These results support the notion that manipulating redox homeostasis by inducing ROS
14
15 could be an efficacious therapeutic strategy.
16
17
18

19
20 Another significant pathway upregulated following 4 hours of QD treatment is the
21
22 unfolded protein response (UPR) (Figure 2). In the ER, where an oxidizing environment is
23
24 required for formation of disulfide bonds, the luminal redox state is under stringent regulation.
25
26 UPR is triggered when there is imbalance between protein-folding demands and protein folding
27
28 capacity, as well as any homeostatic perturbation that can cause protein misfolding, such as
29
30 nutrition deprivation or redox insults.⁷² Furthermore, UPR serves as a sensitive cytoprotective
31
32 response to integrated stresses including oxidative stress. The activation of the NRF2-mediated
33
34 oxidative stress response and UPR both imply that QD232 and QD325 treatments induce
35
36 oxidative stress. While the activation of NRF2 protects cells against ROS, activation of UPR is
37
38 considered to be both an adaptive response and a major executor of cell death in response to
39
40 oxidative stress. UPR regulates cell survival on the basis of the severity and the duration of the
41
42 ER stress. The proapoptotic path of UPR is adopted through several mechanisms including
43
44 induction of CHOP and its transcription targets to activate apoptosis.⁷² Upregulation of CHOP is
45
46 observed following treatment with the QD compounds (Figure 3), suggesting that ER-mediated
47
48 apoptosis is a major mechanism of cytotoxicity of the QD compounds.
49
50
51
52
53
54
55
56
57
58
59
60

1
2
3 For the mitochondrial genome, we observed substantial inhibition of transcription from
4 the HSP2 and LSP promoters (Figure 4), with only modest change in the transcription from the
5 HSP1 promoter (Figure S6). This suggests selectivity in QD-mediated inhibition of transcription.
6
7 The displacement loop (D-loop) is a non-coding control region in the mitochondrial genome
8 where promoters for transcription of the H and L strands (HSP and LSP), as well as the origin of
9 replication (O_H) are located.⁷³ There are two promoters for the H-strand, while transcripts from
10 HSP1 terminates right after the two rRNAs, transcripts from HSP2 cover the full strand and are
11 subjected to subsequent processing into individual mRNA, tRNA and rRNA molecules.^{74, 75} The
12 selective transcriptional inhibition of two out of the three promoters implies that mechanisms
13 other than universal oxidative damaging contribute to such suppressed transcription, and might
14 serve as a pharmacologically induced model to further elucidate regulation of transcription from
15 the mitochondrial genome. We hypothesize that blockage of transcription initiation of selective
16 promoters in the D-loop is a unique feature of the mechanism of action of the QD compounds.
17
18
19
20
21
22
23
24
25
26
27
28
29
30
31
32

33 In our *in vivo* xenograft model for pancreatic cancer, QD325 showed substantial
34 antitumor efficacy with a favorable safety profile. Our original lead compound QD232
35 significantly delayed tumor growth at 20 mg/kg in a similar MIA PaCa-2 xenograft model as
36 reported earlier,²⁹ suppressing growth of tumor by 65% in the 31-day study. QD325, the most
37 potent compound in this lead optimization campaign, showed improved potency by achieving
38 comparable tumor inhibitory effect at a dose of only 5 mg/kg. QD325 did not show any toxicity
39 following repetitive treatments with doses as high as 20 mg/kg, suggesting that it is well
40 tolerated and that it has a favorable therapeutic window. We repeated the experiments with two
41 independent experiments under the same conditions (Figure 5A and Figure 6E), and observed
42 similar results (76% vs. 83% inhibition of tumor growth) for QD325-treated animals.
43
44
45
46
47
48
49
50
51
52
53
54
55
56
57
58
59
60

1
2
3 Gemcitabine is the standard of care treatment for pancreatic cancer patients. In our
4 studies, QD325 showed similar antitumor effect as gemcitabine, supporting the application of
5 QD325 as a novel therapeutic option with a distinct new mechanism, especially for patients with
6 gemcitabine resistance. Due to its remarkable ROS-induction in tumor cells, we expect QD325
7 to be less toxic than gemcitabine. In general, drug combinations demonstrate survival advantages
8 over single-agent therapy as long as they have manageable safety profiles. Our studies show that
9 combination with gemcitabine is tolerable without additional toxicity burden to mice. However,
10 to perform clinically relevant synergy studies both drugs need to be evaluated at optimal doses
11 and in additional cell lines and mice models. These findings warrant the development of QD325
12 as a novel treatment for PDAC as a single agent and in combination with standard of care drugs.
13
14
15
16
17
18
19
20
21
22
23
24
25
26
27
28

29 **CONCLUSIONS**

30
31 In this study, we successfully optimized the anticancer ROS modulator QD232, leading
32 to the discovery of QD325 that shows significant ROS dependent anticancer activity in PDAC
33 models. Bru-seq analysis predicted cellular responses in the nucleus, ER, and mitochondrial for
34 the ROS-mediated cytotoxicity in pancreatic cancer cells, providing in-depth understanding of
35 the unique mechanisms of this active class of anti-cancer compounds. Significant antitumor
36 efficacy and the favorable safety profile of QD325 in vivo provides strong rationale for further
37 developing these QD drugs to target mitochondria as a novel approach to treat PDAC.
38
39
40
41
42
43
44
45
46
47
48
49
50
51
52
53
54
55
56
57
58
59
60

EXPERIMENTAL SECTION

Chemistry

General methods

The reference compound QD232 and the intermediate **6** were prepared as previously described by us (see refs. 30 and 32, respectively). All solvents, including anhydrous solvents, and chemicals, were purchased from Aldrich Co., Alfa Aesar, or Carlo Erba, and were used without further purification. All reactions involving air- or moisture-sensitive compounds were performed under a nitrogen atmosphere using oven-dried glassware and syringes to transfer solutions. Analytical thin-layer chromatography (TLC) was carried out on Merck silica gel F-254 plates. Flash chromatography purifications were performed on Merck Silica gel 60 (230–400 mesh ASTM) as a stationary phase. Melting points (mp) were determined using an Electrothermal melting point or a K \ddot{o} fler apparatus and are uncorrected. Nuclear magnetic resonance (^1H NMR, ^{13}C NMR) spectra were recorded in CDCl_3 or DMSO-d_6 on 400 MHz Bruker Avance III. Chemical shifts (δ) are reported in parts per million (ppm) downfield from tetramethylsilane (TMS), used as an internal standard. Splitting patterns are designated as follows, singlet; d, doublet; t, triplet; q, quadruplet; m, multiplet; brs, broad singlet; dd, double doublet. The assignment of exchangeable protons (OH and NH) was confirmed by the addition of D_2O . Mass spectra were obtained on a Hewlett-Packard 5989 mass engine spectrometer, or a MALDI micro MX (Waters, Micromass) equipped with a reflectron analyzer. Elemental analyses were performed on a Perkin-Elmer Elemental Analyzer 2400-CHN at Laboratory of Microanalysis, Department of Chemistry and Pharmacy, University of Sassari (Italy), and were within $\pm 0.4\%$ of the theoretical values (Table S8), thus confirming $\geq 95\%$ purity.

1
2
3 **General Method A: Preparation of Compounds QD324-327, 329, 331, 332, 334-336,**
4
5 **338, 353-357.** A solution of quinazoline-5,8-dione, cerium (III) chloride heptahydrate ($\text{CeCl}_3 \cdot 7$
6 H_2O , 1.1 eq.) and (3,4,5)-substituted aniline (1.1 eq.) in absolute ethanol was stirred at room
7
8 temperature for 1-2 h. Next, most of the ethanol was removed under vacuum, and water was
9
10 added, followed by the extraction with CH_2Cl_2 . The organic layers were washed with water and
11
12 brine, dried over anhydrous Na_2SO_4 and concentrated to dryness. Then, the crude product was
13
14 purified by flash chromatography to give the expected product.
15
16
17
18
19
20
21

22 **General Method B: Preparation of the Compounds QD328, 330, 333, 337.** A solution
23
24 of quinazoline-5,8-dione, cerium (III) chloride heptahydrate ($\text{CeCl}_3 \cdot 7 \text{H}_2\text{O}$, 1.1 eq.) and (3,4,5)-
25
26 substituted aniline (1.1 eq.) in absolute ethanol was stirred at room temperature for 2-6 h. Next,
27
28 most of the ethanol was removed under vacuum, and water was added, followed by the
29
30 extraction with CH_2Cl_2 . The organic layers were dried over sodium sulfate (Na_2SO_4) and
31
32 concentrated to dryness. Then, the crude residue was treated with water, and the solid residue
33
34 that precipitated was filtered and triturated with petroleum ether to give the desired product.
35
36
37
38
39
40

41 **3,6-Dimethoxy-2-nitrobenzaldehyde (2).** Nitric acid (8.0 mL; 179.02 mmol), acetic
42
43 anhydride (8.0 mL, 84.24 mmol) and 2,5-dimethoxybenzaldehyde (**1**, 4.0 g, 24.07 mmol) were
44
45 added at 0 °C with stirring, respectively. After 1.5 h stirring, the mixture was poured onto 20 mL
46
47 ice/water. The resultant yellow solid was filtered, washed with cold water and then purified by
48
49 flash chromatography on silica gel using ethyl acetate-petroleum ether (1:1) to give first the
50
51 regioisomer 2,5-dimethoxy-4-nitrobenzaldehyde, and then (by further elution with only ethyl
52
53 acetate) the desired compound **2**. Yield: 68%. R_f = 0.10 (ethyl acetate-petroleum ether 5:5); mp:
54
55
56
57
58
59
60

1
2
3 167 °C. ¹H-NMR 400 MHz (DMSO-d₆): δ 10.25 (s, 1H), 7.70 (d, 1H), 7.48 (d, 1H), 3.95 (s, 3H),
4
5 3.86 (s, 3H). ¹H-NMR 400 MHz (CDCl₃): δ 10.39 (s, 1H), 7.30 (d, 1H), 7.12 (d, 1H), 3.97 (s,
6
7 3H), 3.89 (s, 3H). MS: *m/z* 211 [M]⁺.
8
9

10
11
12 **N,N'-[(3,6-dimethoxy-2-nitrophenyl)methanediyl]diformamide (3)**. A solution of 3,6-
13
14 dimethoxy-2-nitrobenzaldehyde (**2**, 11.90 g, 56.35 mmol) in formamide (66.5 eq., 150 mL),
15
16 heated at 40 °C, was exposed to dry HCl gas (1 h) until the temperature reached 80 °C. Then, the
17
18 solution was cooled to room temperature, and water/ice was added. Pale yellow colored
19
20 precipitate was formed, which was filtered, dried and triturated with ethyl acetate and petroleum
21
22 ether to yield the desired compound. Yield: 90%. R_f= 0.26 (dichloromethane-methanol 9.5:0.5);
23
24 mp: 255 °C. ¹H-NMR 400 MHz (DMSO-d₆): δ 8.67 (d, 2H), 7.92 (s, 2H), 7.28 (s, 2H), 6.77 (t,
25
26 1H), 3.88 (s, 3H), 3.82 (s, 3H). MS: *m/z* 283 [M]⁺.
27
28
29
30
31
32

33 **5,8-Dimethoxyquinazoline (4)**. Zinc powder (22.9 g) was added to a suspension of
34
35 N,N'-[(3,6-dimethoxy-2-nitrophenyl)methanediyl]diformamide (**3**, 7.0 g, 24.71 mmol) in
36
37 triturated ice (92 g) and glacial acetic acid (32 mL), under constant magnetic stirring. The
38
39 reaction mixture was stirred for 2 h in ice bath, and for 4 h at room temperature. After filtration
40
41 of the reaction mixture through filter paper, the resulting solution was dropped on cooled 50%
42
43 NaOH (120 mL) and the yellow colored suspension thus formed was left without stirring for 1 h.
44
45 Next, the suspension was filtered and the solid dried (at 30-40 °C) to give a yellow powder. The
46
47 solid was then solubilized in ethyl acetate, filtered, dried over anhydrous Na₂SO₄, and
48
49 concentrated to dryness yielding the desired compound. Yield: 79%. R_f= 0.46 (dichloromethane-
50
51
52
53
54
55
56
57
58
59
60

1
2
3 methanol 9.5:0.5); mp: 106 °C. ¹H-NMR 400 MHz (DMSO-d₆): δ 9.64 (s, 1H), 9.28 (s, 1H), 7.39
4
5 (d, 1H), 7.10 (d, 1H), 3.98 (s, 3H), 3.94 (s, 3H). MS: *m/z* 190 [M]⁺
6
7
8
9

10 **(3-Aminopropyl)triphenylphosphonium bromide hydrobromide (6)**. To a 50 mL
11 round-bottom flask equipped with a magnetic stirring bar, triphenylphosphine (1.0 eq., 1.0 g, 3.82
12 mmol), 3-bromopropylamine hydrobromide (**5**, 1.0 eq., 0.84 g, 3.82 mmol), and acetonitrile (7
13 mL), were added. The resulting suspension was heated to reflux and the mixture was stirred for
14 16 h. The reaction was cooled to room temperature, then n-hexane was added and the resulting
15 solid was filtered, washed with n-hexane, dissolved in 100 mL isopropanol and precipitated with
16 cold diethyl ether, to give a white powder. Yield: 50%; R_f= 0.28 (dichlorometane-methanol 9:1);
17 mp: 200 °C. ¹H-NMR 400 MHz (CDCl₃): δ 7.95-7.92 (m, 3H), 7.84-7.74 (m, 15 H), 3.74 (m,
18 2H), 3.00-2.98 (m, 2H), 1.85 (m, 2H).
19
20
21
22
23
24
25
26
27
28
29
30
31
32

33 **Quinazoline-5,8-dione (QD323)**. A solution of 5,8-dimethoxyquinazoline (**4**, 0.35 g,
34 1.84 mmol) in (7:3) acetonitrile:water (10 mL) was cooled at 0 °C in an ice bath and a solution
35 of ceric ammonium nitrate (2.7 eq., 2.72 g, 4.97 mmol) in (9:1) acetonitrile:water (10 mL) was
36 added dropwise. The reaction mixture was stirred for 20 minutes, then poured into ice/water and
37 extracted (8-10 times) with CH₂Cl₂. The organic layer was washed (5-6 times) with water, dried
38 over anhydrous Na₂SO₄ and concentrated to dryness to give a brown powder. Yield: 69%. R_f=
39 0.62 (dichloromethane-methanol 9.5:0.5); mp: > 320 °C. ¹H-NMR 400 MHz (DMSO-d₆): δ 9.69
40 (s, 1H), 9.43 (s, 1H), 7.28 (d, 1H), 7.18 (d, 1H). ¹³C-NMR 400 MHz (DMSO-d₆): δ 184.07,
41 182.88, 162.08, 156.27, 152.61, 139.46, 137.74, 124.61. MS: *m/z* 160 [M]⁺
42
43
44
45
46
47
48
49
50
51
52
53
54
55
56
57
58
59
60

1
2
3 **6-((4-Phenoxyphenyl)amino)quinazoline-5,8-dione (QD324).** Quinazoline-5,8-dione
4
5 (**QD323**, 0.10 g, 0.62 mmol), cerium (III) chloride heptahydrate ($\text{CeCl}_3 \cdot 7 \text{H}_2\text{O}$, 1.1 eq., 0.26 g,
6
7 0.69 mmol), 4-phenoxyaniline (1.1 eq., 0.13 g, 0.69 mmol), and absolute ethanol (11 mL). Flash
8
9 chromatography (ethyl acetate-petroleum ether 6:4) gave compound **QD324** as a violet powder.
10
11 Yield: 65%. $R_f = 0.30$ (ethyl acetate-petroleum ether 6:4); mp: 169-171 °C. $^1\text{H-NMR}$ 400 MHz
12
13 (CDCl_3): δ 9.66 (s, 1H), 9.49 (s, 1H), 7.51 (s, 1H), 7.39 (t, 2H), 7.25 (d, 2H), 7.20-7.15 (m, 1H),
14
15 7.09-7.04 (m, 4H), 6.53 (s, 1H). $^{13}\text{C-NMR}$ 400 MHz (CDCl_3): δ 180.65, 180.39, 163.76, 156.48,
16
17 156.31, 154.40, 145.15, 130.90, 130.01, 125.25, 124.04, 123.34, 119.76, 119.28, 104.65. MS:
18
19 m/z 343 $[\text{M}]^+$
20
21
22
23
24
25

26 **6-([1,1'-Biphenyl]-4-ylamino)quinazoline-5,8-dione (QD325).** Quinazoline-5,8-dione
27
28 (**QD323**, 0.16 g, 1.01 mmol), cerium (III) chloride heptahydrate ($\text{CeCl}_3 \cdot 7 \text{H}_2\text{O}$, 1.1 eq., 0.41 g,
29
30 1.11 mmol), 4-aminobiphenyl (1.1 eq., 0.19 g, 1.11 mmol), and absolute ethanol (19 mL). Flash
31
32 chromatography (ethyl acetate-petroleum ether 7:3) gave compound **QD325** as a violet powder.
33
34 Yield: 58%. $R_f = 0.48$ (ethyl acetate-petroleum ether 8:2); mp: 230 °C. $^1\text{H-NMR}$ 400 MHz
35
36 (CDCl_3): δ 9.68 (s, 1H), 9.51 (s, 1H), 7.68 (d, 2H), 7.65 (s, 1H), 7.60 (d, 2H), 7.48 (t, 2H), 7.42-
37
38 7.36 (m, 3H), 6.73 (s, 1H). $^{13}\text{C-NMR}$ 400 MHz (CDCl_3): δ 180.67, 180.52, 163.78, 156.39,
39
40 154.32, 144.33, 139.71, 135.44, 128.99, 128.53, 127.53, 127.00, 123.26, 105.20. MS: m/z 327
41
42
43
44
45 $[\text{M}]^+$
46
47
48
49

50 **6-((3,4,5-Trimethoxyphenyl)amino)quinazoline-5,8-dione (QD326).** Quinazoline-5,8-
51
52 dione (**QD323**, 0.07 g, 0.44 mmol), cerium (III) chloride heptahydrate ($\text{CeCl}_3 \cdot 7 \text{H}_2\text{O}$, 1.1 eq.,
53
54 0.18 g, 0.48 mmol), 3,4,5-trimethoxyaniline (1.1 eq., 0.09 g, 0.48 mmol), and absolute ethanol (8
55
56
57
58
59
60

mL). Flash chromatography (ethyl acetate-petroleum ether from 7:3 to 8:2) gave compound **QD326** as a violet powder. Yield: 88%. Rf= 0.18 (ethyl acetate-petroleum ether 8:2); mp: 161-162 °C. ¹H-NMR 400 MHz (CDCl₃): δ 9.67 (s, 1H), 9.49 (s, 1H), 7.51 (s, 1H), 6.59 (s, 1H), 6.50 (s, 2H), 3.88 (s, 9H). ¹³C-NMR 400 MHz (CDCl₃): δ 180.61, 180.40, 163.77, 156.33, 154.15, 144.90, 136.96, 131.87, 123.30, 105.00, 101.20, 61.07, 56.39. MS: *m/z* 341 [M]⁺

6-((4-(Trifluoromethoxy)phenyl)amino)quinazoline-5,8-dione (QD327). Quinazoline-5,8-dione (**QD323**, 0.05 g, 0.31 mmol), cerium (III) chloride heptahydrate (CeCl₃·7 H₂O, 1.1 eq., 0.13 g, 0.34 mmol), 4-(trifluoromethoxy)aniline (1.1 eq., 0.046 mL, 0.34 mmol), and absolute ethanol (6 mL). Flash chromatography (dichloromethane-methanol 9.7:0.3) gave compound **QD327** as a dark red powder. Yield: 67%. Rf= 0.53 (dichloromethane-methanol 9.5:0.5); mp: 114 °C. ¹H-NMR 400 MHz (CDCl₃): δ 9.68 (s, 1H), 9.51 (s, 1H), 7.55 (s, 1H), 7.33 (s, 4H), 6.58 (s, 1H). MS: *m/z* 335 [M]⁺

4-((5,8-Dioxo-5,8-dihydroquinazolin-6-yl)amino)benzenesulfonamide (QD328). Quinazoline-5,8-dione (**QD323**, 0.05 g, 0.31 mmol), cerium (III) chloride heptahydrate (CeCl₃·7 H₂O, 1.1 eq., 0.13 g, 0.34 mmol), sulfanilamide (1.1 eq., 0.06 g, 0.34 mmol), and absolute ethanol (6 mL). The precipitate was filtered and triturated with petroleum ether gave compound **QD328** as a red powder. Yield: 59%. Rf= 0.16 (ethyl acetate-petroleum ether 8:2); mp: >320 °C. ¹H-NMR 400 MHz (DMSO-d₆): δ 9.72 (s, 1H), 9.64 (s, 1H), 9.44 (s, 1H), 7.88 (d, 2H), 7.60 (d, 2H), 7.38 (s, 2H), 6.46 (s, 1H). ¹³C-NMR 400 MHz (DMSO-d₆): δ 180.50, 180.32, 162.58, 155.78, 153.46, 145.33, 140.91, 140.20, 127.38, 127.05, 124.19, 123.17, 112.38, 105.11. MS: *m/z* 331 [M+1]⁺

1
2
3
4
5
6 **6-((4-(Hydroxymethyl)phenyl)amino)quinazoline-5,8-dione (QD329).** Quinazoline-
7
8 5,8-dione (**QD323**, 0.05 g, 0.31 mmol), cerium (III) chloride heptahydrate ($\text{CeCl}_3 \cdot 7 \text{H}_2\text{O}$, 1.1
9
10 eq., 0.13 g, 0.34 mmol), 4-aminobenzyl alcohol (1.1 eq., 0.04 g, 0.34 mmol), and absolute
11
12 ethanol (6 mL). Flash chromatography (dichloromethane-methanol 9.7:0.3) gave compound
13
14 **QD329** as a brown-red powder. Yield: 27%. $R_f = 0.30$ (dichloromethane-methanol 9.5:0.5); mp:
15
16 203 °C. $^1\text{H-NMR}$ 400 MHz (CDCl_3): δ 9.67 (s, 1H), 9.50 (s, 1H), 7.59 (s, 1H), 7.47 (d, 2H), 7.29
17
18 (d, 2H), 6.64 (s, 1H), 4.75 (s, 2H). MS: m/z 303 $[\text{M}+\text{Na}]^+$
19
20
21
22
23

24 **4-((5,8-Dioxo-5,8-dihydroquinazolin-6-yl)amino)benzamide (QD330).** Quinazoline-
25
26 5,8-dione (**QD323**, 0.05 g, 0.31 mmol), cerium (III) chloride heptahydrate ($\text{CeCl}_3 \cdot 7 \text{H}_2\text{O}$, 1.1
27
28 eq., 0.13 g, 0.34 mmol), 4-aminobenzamide (1.1 eq., 0.05 g, 0.34 mmol), and absolute ethanol (6
29
30 mL). The precipitate was filtered and triturated with petroleum ether gave compound **QD330** as
31
32 a brown powder. Yield: 24%. $R_f = 0.58$ (dichloromethane-methanol 9.5:0.5); mp: > 320 °C. $^1\text{H-}$
33
34 NMR 400 MHz (DMSO-d_6): δ 9.65 (s, 1H), 9.63 (s, 1H), 9.43 (s, 1H), 7.95 (d, 2H), 7.49 (d, 2H),
35
36 7.38 (s, 2H), 6.42 (s, 1H). MS: m/z 295 $[\text{M}+1]^+$
37
38
39
40
41
42

43 **Methyl 4-((5,8-dioxo-5,8-dihydroquinazolin-6-yl)amino)benzoate (QD331).**
44
45 Quinazoline-5,8-dione (**QD323**, 0.06 g, 0.37 mmol), cerium (III) chloride heptahydrate ($\text{CeCl}_3 \cdot$
46
47 $7 \text{H}_2\text{O}$, 1.1 eq., 0.15 g, 0.41 mmol), methyl 4-aminobenzoate (1.1 eq., 0.06 g, 0.41 mmol), and
48
49 absolute ethanol (7.2 mL). Flash chromatography (ethyl acetate-petroleum ether from 6:4 to 7:3)
50
51 gave compound **QD331** as a red powder. Yield: 42%. $R_f = 0.35$ (ethyl acetate-petroleum ether
52
53 7:3); mp: 226-230 °C. $^1\text{H-NMR}$ 400 MHz (CDCl_3): δ 9.69 (s, 1H), 9.52 (s, 1H), 8.14 (d, 2H),
54
55
56
57
58
59
60

1
2
3 7.72 (s, 1H), 7.36 (d, 2H), 6.81 (s, 1H), 3.95 (s, 3H). ¹³C-NMR 400 MHz (CDCl₃): δ 180.75,
4 180.40, 165.96, 163.85, 156.57, 153.96, 143.34, 140.64, 131.51, 127.69, 123.27, 121.66, 121.55,
5 106.35, 52.35. MS: *m/z* 309 [M]⁺
6
7
8
9

10
11
12 **Ethyl 4-((5,8-dioxo-5,8-dihydroquinazolin-6-yl)amino)benzoate (QD332).**
13

14 Quinazoline-5,8-dione (**QD323**, 0.13 g, 0.81 mmol), cerium (III) chloride heptahydrate (CeCl₃·
15 7 H₂O, 1.1 eq., 0.33 g, 0.89 mmol), ethyl 4-aminobenzoate (1.1 eq., 0.15 g, 0.89 mmol), and
16 absolute ethanol (16 mL). Flash chromatography (ethyl acetate-petroleum ether 6.5:3.5) gave
17 compound **QD332** as a red powder. Yield: 39%. R_f= 0.36 (ethyl acetate-petroleum ether 7:3);
18 mp: 206-207 °C. ¹H-NMR 400 MHz (CDCl₃): δ 9.69 (s, 1H), 9.52 (s, 1H), 8.14 (d, 2H), 7.72 (s,
19 1H), 7.36 (d, 2H), 6.80 (s, 1H), 4.43-4.38 (q, 2H), 1.42 (t, 3H). ¹³C-NMR 400 MHz (CDCl₃): δ
20 180.74, 180.42, 165.49, 163.85, 156.56, 153.98, 143.38, 140.53, 131.47, 128.08, 123.27, 121.65,
21 106.31, 61.31, 14.34. MS: *m/z* 323 [M]⁺
22
23
24
25
26
27
28
29
30
31
32
33
34
35

36 **(3-((5,8-Dioxo-5,8-dihydroquinazolin-6-yl)amino)phenyl)boronic acid (QD333).**
37

38 Quinazoline-5,8-dione (**QD323**, 0.05 g, 0.31 mmol), cerium (III) chloride heptahydrate (CeCl₃·
39 7 H₂O, 1.1 eq., 0.13 g, 0.34 mmol), 3-aminophenylboronic acid (1.1 eq., 0.05 g, 0.34 mmol), and
40 absolute ethanol (6 mL). The precipitate was filtered and triturated with petroleum ether gave
41 compound **QD333** as a red powder. Yield: 48%. R_f= 0.37 (dichloromethane-methanol 9.5:0.5);
42 mp: 208-210 °C. ¹H-NMR 400 MHz (DMSO-*d*₆): δ 9.61 (s, 1H), 9.52 (s, 1H), 9.41 (s, 1H), 8.20
43 (s, 2H), 7.77-7.70 (m, 2H), 7.43 (m, 2H), 6.23 (s, 1H). MS: *m/z* 318 [M+Na]⁺
44
45
46
47
48
49
50
51
52
53
54
55
56
57
58
59
60

6-((4'-Fluoro-[1,1'-biphenyl]-4-yl)amino)quinazoline-5,8-dione (QD334).

Quinazoline-5,8-dione (**QD323**, 0.05 g, 0.31 mmol), cerium (III) chloride heptahydrate ($\text{CeCl}_3 \cdot 7 \text{H}_2\text{O}$, 1.1 eq., 0.13 g, 0.34 mmol), 4-amino-4'-fluorobiphenyl (1.1 eq., 0.06 g, 0.34 mmol), and absolute ethanol (6 mL). Flash chromatography (ethyl acetate-petroleum ether from 7:3 to 8:2) gave compound **QD334** as a violet powder. Yield: 29%. $R_f = 0.32$ (ethyl acetate-petroleum ether 7:3); mp: 285-289 °C. $^1\text{H-NMR}$ 400 MHz (CDCl_3): δ 9.68 (s, 1H), 9.51 (s, 1H), 7.63 (d, 2H), 7.55 (t, 2H), 7.53 (s, 1H), 7.37 (d, 2H), 7.16 (t, 2H), 6.72 (s, 1H). $^{13}\text{C-NMR}$ 400 MHz (CDCl_3): δ 180.64, 180.53, 163.97, 163.79, 161.51, 156.39, 154.30, 144.33, 138.70, 135.98, 135.47, 128.65, 128.39, 123.33, 116.03, 115.82, 105.21. MS: m/z 345 $[\text{M}]^+$

6-((4'-Ethyl-[1,1'-biphenyl]-4-yl)amino)quinazoline-5,8-dione (QD335).

Quinazoline-5,8-dione (**QD323**, 0.05 g, 0.34 mmol), cerium (III) chloride heptahydrate ($\text{CeCl}_3 \cdot 7 \text{H}_2\text{O}$, 1.1 eq., 0.14 g, 0.37 mmol), 4-amino-4'-ethylbiphenyl (1.1 eq., 0.07 g, 0.37 mmol), and absolute ethanol (6.5 mL). Flash chromatography (ethyl acetate-petroleum ether from 6:4 to 7:3) gave compound **QD335** as a red-violet powder. Yield: 60%. $R_f = 0.36$ (ethyl acetate-petroleum ether 7:3); mp: 232 °C. $^1\text{H-NMR}$ 400 MHz (CDCl_3): δ 9.66 (s, 1H), 9.49 (s, 1H), 7.68 (s, 1H), 7.66 (d, 2H), 7.51 (d, 2H), 7.34 (d, 2H), 7.30 (d, 2H), 6.71 (s, 1H), 2.74-2.68 (q, 2H), 1.29 (t, 3H). $^{13}\text{C-NMR}$ 400 MHz (CDCl_3): δ 180.67, 180.48, 163.73, 156.35, 154.34, 144.35, 144.09, 139.64, 137.03, 135.15, 128.53, 128.46, 126.89, 123.35, 123.24, 105.11, 28.54, 15.55. MS: m/z 356 $[\text{M}+1]^+$

6-((4'-Methoxy[1,1'-biphenyl]-4-yl)amino)quinazoline-5,8-dione (QD336).

Quinazoline-5,8-dione (**QD323**, 0.05 g, 0.34 mmol), cerium (III) chloride heptahydrate ($\text{CeCl}_3 \cdot$

1
2
3 7 H₂O, 1.1 eq., 0.14 g, 0.37 mmol), 4'-methoxy-biphenyl-4-ylamine (1.1 eq., 0.07 g, 0.37 mmol),
4 and absolute ethanol (6.5 mL). Flash chromatography (ethyl acetate-petroleum ether from 7:3 to
5 10:0) gave compound **QD336** as a dark violet powder. Yield: 69%. R_f= 0.29 (ethyl acetate-
6 petroleum ether 7:3); mp: 270-272 °C. ¹H-NMR 400 MHz (CDCl₃): δ 9.67 (s, 1H), 9.51 (s, 1H),
7 7.63 (d, 2H), 7.61 (s, 1H), 7.53 (d, 2H), 7.32 (d, 2H), 7.01 (d, 2H), 6.71 (s, 1H), 3.87 (s, 3H).
8 ¹³C-NMR 400 MHz (CDCl₃): δ 180.67, 180.47, 163.77, 159.58, 156.36, 154.37, 144.38, 139.38,
9 134.81, 132.20, 128.05, 128.01, 123.29, 123.19, 114.44, 105.09, 55.40. MS: *m/z* 357 [M]⁺
10
11
12
13
14
15
16
17
18
19
20

21 **6-((4'-Amino-[1,1'-biphenyl]-4-yl)amino)quinazoline-5,8-dione (QD337).**

22 Quinazoline-5,8-dione (**QD323**, 0.05 g, 0.34 mmol), cerium (III) chloride heptahydrate (CeCl₃·
23 7 H₂O, 1.1 eq., 0.14 g, 0.37 mmol), benzidine (1.1 eq., 0.07 g, 0.37 mmol), and absolute ethanol
24 (6.5 mL). The precipitate was filtered and triturated with petroleum ether gave compound
25 **QD337** as a dark violet powder. Yield: 16%. R_f= 0.71 (dichlorometane-methanol 9.5:0.5); mp:
26 >320 °C. ¹H-NMR 400 MHz (DMSO-d₆): δ 9.66 (s, 1H), 9.63 (s, 1H), 9.44 (s, 1H), 7.83 (d, 2H),
27 7.64 (d, 1H), 7.53 (d, 2H), 7.40 (d, 2H), 6.65 (d, 1H), 6.40 (s, 1H), 5.27 (s, 2H). MS: *m/z* 342
28 [M]⁺
29
30
31
32
33
34
35
36
37
38
39
40
41

42 **6-((2-Fluoro-4'-methyl-[1,1'-biphenyl]-4-yl)amino)quinazoline-5,8-dione (QD338).**

43 Quinazoline-5,8-dione (**QD323**, 0.06 g, 0.35 mmol), cerium (III) chloride heptahydrate (CeCl₃·
44 7 H₂O, 1.1 eq., 0.14 g, 0.38 mmol), 2-fluoro-4'-methyl-biphenyl-4-ylamine (1.1 eq., 0.08 g, 0.38
45 mmol), and absolute ethanol (6.7 mL). Flash chromatography (ethyl acetate-petroleum ether,
46 from 6:4 to 8:2) gave compound **QD338** as a violet powder. Yield: 60%. R_f= 0.26 (ethyl acetate-
47 petroleum ether 7:3); mp: 282-283 °C. ¹H-NMR 400 MHz (CDCl₃): δ 9.69 (s, 1H), 9.52 (s, 1H),
48
49
50
51
52
53
54
55
56
57
58
59
60

1
2
3 7.62 (s, 1H), 7.52 (t, 1H), 7.45 (d, 2H), 7.29 (d, 2H), 7.14 (t, 2H), 6.75 (s, 1H), 2.42 (s, 3H). ¹³C-
4 NMR 400 MHz (CDCl₃): δ 180.61, 180.47, 163.83, 156.49, 143.93, 138.14, 131.79, 129.40,
5
6 128.89, 128.71, 123.31, 118.67, 110.85, 110.58, 105.75, 21.24. MS: *m/z* 359 [M]⁺
7
8
9

10
11
12 **(3-(4-Aminobenzamido)propyl)triphenylphosphonium bromide (QD339)**. To a solution of 4-
13 aminobenzoic acid (1.0 eq., 0.076 g, 0.55 mmol) in CH₂Cl₂ (12 mL), *N,N*-diisopropylethylamine
14 (DIPEA, 5 eq. 0.48 mL, 2.75 mmol), and HBtU (1.0 eq., 0.206 g, 0.55 mmol) were added. The
15 reaction mixture was stirred for 15 minutes, and (3-aminopropyl)triphenylphosphonium bromide
16 (**6**, 3 eq. 0.80 g, 1.66 mmol) and DMAP (0.04 eq., 2.7 μg, 0.02 mmol) were added. The resulting
17 mixture was stirred at room temperature for 5 h, filtered, washed with CH₂Cl₂, and concentrated
18 to dryness. The crude product was purified by flash chromatography on silica gel using
19 dichloromethane-isopropanol (9.5:0.5) to give **QD339** as a beige powder. Yield: 70%; R_f= 0.27
20 (dichloromethane-methanol 9:1); mp: 203-205 °C. ¹H-NMR 400 MHz (CDCl₃): δ 8.91 (t, 1H),
21 8.10 (d, 2H), 7.77-7.72 (m, 9H), 7.61-7.58 (m, 6H), 6.70 (d, 2H), 3.94-3.90 (m, 2H), 3.72-3.71
22 (m, 2H), 1.95 (m, 2H). MS: *m/z* 439.
23
24
25
26
27
28
29
30
31
32
33
34
35
36
37
38
39

40 **(3-(4-((5,8-Dioxo-5,8-dihydroquinazolin-6-yl)amino)benzamido)propyl)**
41 **triphenylphosphonium bromide (QD340)**. A solution of quinazoline-5,8-dione (**5**, 1.0 eq., 0.04
42 g, 0.25 mmol), cerium (III) chloride heptahydrate (CeCl₃·7 H₂O, 1.1 eq., 0.102 g, 0.27 mmol)
43 and (3-(4-aminobenzamido)propyl)triphenylphosphonium bromide (**QD339**, 1.1 eq., 0.143 g,
44 0.27 mmol) in absolute ethanol (5 mL) was stirred at room temperature for 2 h. Then, most of the
45 ethanol was removed under vacuum, and water was added, followed by the extraction with
46 CH₂Cl₂. The organic layers were washed with water, brine, dried over anhydrous sodium
47
48
49
50
51
52
53
54
55
56
57
58
59
60

1
2
3 sulphate and concentrated to dryness. The crude product was triturated with petroleum ether to
4 give **QD340** as a red powder. Yield: 42%; Rf= 0.45 (dichlorometane-methanol 9:1); mp: 205 °C.
5
6 ¹H-NMR 400 MHz (CDCl₃): δ 9.90 (t, 1H), 9.67 (s, 1H), 9.50 (s, 1H), 8.46 (d, 2H), 7.79-7.72 (m,
7
8 10H), 7.65-7.62 (m, 6H), 7.37 (d, 2H), 6.74 (s, 1H), 3.97-3.93 (m, 2H), 3.75-3.74 (m, 2H), 2.00
9
10 (m, 2H). MS: *m/z* 597.
11
12
13
14
15
16

17 **6-((3-Methoxyphenyl)amino)quinazoline-5,8-dione (QD353)**. Quinazoline-5,8-dione
18
19 (**QD323**, 0.05 g, 0.31 mmol), cerium (III) chloride heptahydrate (CeCl₃·7 H₂O, 1.1 eq., 0.13 g,
20
21 0.34 mmol), *m*-anisidine (1.1 eq., 0.38 mL, 0.34 mmol), and absolute ethanol (6 mL). Flash
22
23 chromatography (ethyl acetate-petroleum ether 6:4) gave compound **QD353** as a dark violet
24
25 powder. Yield: 43%. Rf= 0.30 (ethyl acetate-petroleum ether 7:3); mp: 142 °C. ¹H-NMR 400
26
27 MHz (CDCl₃): δ 9.67 (s, 1H), 9.50 (s, 1H), 7.56 (s, 1H), 7.36 (t, 1H), 6.88 (d, 2H), 6.83 (d, 2H),
28
29 6.82 (s, 1H), 6.69 (s, 1H), 3.84 (s, 3H). ¹³C-NMR 400 MHz (CDCl₃): δ 180.65, 180.56, 163.76,
30
31 160.81, 156.36, 154.28, 144.45, 137.40, 130.75, 123.33, 115.25, 112.07, 109.17, 105.34, 55,53.
32
33 MS: *m/z* 281 [M]⁺
34
35
36
37
38
39

40 **6-((4-Methoxyphenyl)amino)quinazoline-5,8-dione (QD354)**. Quinazoline-5,8-dione
41
42 (**QD323**, 0.06 g, 0.37 mmol), cerium (III) chloride heptahydrate (CeCl₃·7 H₂O, 1.1 eq., 0.15 g,
43
44 0.41 mmol), *p*-anisidine (1.1 eq., 0.05 g, 0.41 mmol), and absolute ethanol (7.2 mL). Flash
45
46 chromatography (ethyl acetate-petroleum ether from 6.5:3.5 to 8:2) gave compound **QD354** as a
47
48 dark powder. Yield: 41%. Rf= 0.32 (ethyl acetate-petroleum ether 7:3); mp: 238 °C. ¹H-NMR
49
50 400 MHz (CDCl₃): δ 9.66 (s, 1H), 9.48 (s, 1H), 7.49 (s, 1H), 7.21 (d, 2H), 6.98 (d, 2H), 6.48 (s,
51
52
53
54
55
56
57
58
59
60

1
2
3 1H), 3.85 (s, 3H). ¹³C-NMR 400 MHz (CDCl₃): δ 180.76, 180.28, 163.73, 156.24, 154.52,
4
5 145.34, 128.75, 125.18, 123.36, 115.16, 104.34, 55,62. MS: *m/z* 281 [M]⁺
6
7
8
9

10 **6-((3,4-Dimethoxyphenyl)amino)quinazoline-5,8-dione (QD355)**. Quinazoline-5,8-
11
12 dione (**QD323**, 0.06 g, 0.40 mmol), cerium (III) chloride heptahydrate (CeCl₃·7 H₂O, 1.1 eq.,
13
14 0.16 g, 0.44 mmol), 3,4-dimethoxyaniline (1.1 eq., 0.067 g, 0.44 mmol), and absolute ethanol
15
16 (7.6 mL). Flash chromatography (ethyl acetate-petroleum ether from 7:3 to 10:0) gave compound
17
18 **QD355** as a dark powder. Yield: 70%. R_f= 0.23 (ethyl acetate-petroleum ether 8:2); mp: 241-
19
20 242 °C. ¹H-NMR 400 MHz (CDCl₃): δ 9.66 (s, 1H), 9.49 (s, 1H), 7.50 (s, 1H), 6.92 (d, 2H), 6.86
21
22 (d, 2H), 6.78 (s, 1H), 6.53 (s, 1H), 3.92 (s, 3H), 3.90 (s, 3H). ¹³C-NMR 400 MHz (CDCl₃): δ
23
24 180.73, 180.31, 163.75, 156.75, 156.26, 154.48, 149.97, 148.10, 145.21, 129.02, 123.34, 116.10,
25
26 111.74, 107.50, 104.54, 56,18. MS: *m/z* 334 [M+Na]⁺
27
28
29
30
31
32

33 **6-((4-Fluorobenzyl)amino)quinazoline-5,8-dione (QD356)**. Quinazoline-5,8-dione
34
35 (**QD323**, 0.06 g, 0.40 mmol), cerium (III) chloride heptahydrate (CeCl₃·7 H₂O, 1.1 eq., 0.16 g,
36
37 0.44 mmol), 4-fluorobenzylamine (1.1 eq., 0.05 mL, 0.44 mmol), and absolute ethanol (7.6 mL).
38
39 Flash chromatography (ethyl acetate-petroleum ether from 7:3 to 8:2) gave compound **QD356** as
40
41 an orange powder. Yield: 35%. R_f= 0.30 (ethyl acetate-petroleum ether 8:2); mp: 203 °C. ¹H-
42
43 NMR 400 MHz (CDCl₃): δ 9.64 (s, 1H), 9.43 (s, 1H), 7.30 (t, 2H), 7.09 (t, 2H), 6.28 (s, 1H),
44
45 6.05 (s, 1H), 4.40 (d, 2H). ¹³C-NMR 400 MHz (CDCl₃): δ 180.33, 179.62, 163.93, 163.67,
46
47 161.47, 156.16, 154.57, 146.96, 130.68, 129.43, 123.35, 116.14, 103.76, 46.30. MS: *m/z* 283
48
49
50
51 [M]⁺
52
53
54
55
56
57
58
59
60

1
2
3 **6-((3,5-Dimethoxyphenyl)amino)quinazoline-5,8-dione (QD357).** Quinazoline-5,8-dione
4 **(QD323,** 0.06 g, 0.40 mmol), cerium (III) chloride heptahydrate ($\text{CeCl}_3 \cdot 7 \text{H}_2\text{O}$, 1.1 eq., 0.16 g,
5 0.44 mmol), 3,5-dimethoxyaniline (1.0 eq., 0.07 g, 0.44 mmol), and absolute ethanol (7.6 mL).
6
7
8
9
10 Flash chromatography (ethyl acetate-petroleum ether from 6:4 to 7:3) gave compound **QD357** as
11 a violet powder. Yield: 70%. Rf= 0.45 (ethyl acetate-petroleum ether 8:2); mp: 204-206 °C. ^1H -
12 NMR 400 MHz (DMSO-d_6): δ 9.66 (s, 1H), 9.43 (s, 1H), 7.05 (s, 1H), 5.97 (s, 2H), 5.72 (s, 2H),
13 3.62 (s, 6H). ^{13}C -NMR 400 MHz (CDCl_3): δ 183.14, 182.27, 162.43, 159.30, 157.54, 152.64,
14 150.43, 145.40, 138.54, 125.32, 100.99, 91.24, 55,74. MS: m/z 312 $[\text{M}+1]^+$
15
16
17
18
19
20
21
22
23

24 **(3-(3-Aminobenzamido)propyl)triphenylphosphonium bromide (QD358).** To a
25 solution of 3-aminobenzoic acid (1.0 eq., 0.076 g, 0.55 mmol) in CH_2Cl_2 (12 mL), *N,N*-
26 diisopropylethylamine (DIPEA, 5 eq. 0.48 mL, 2.75 mmol), and HBTU (1.0 eq., 0.206 g, 0.55
27 mmol) were added. The reaction mixture was stirred for 15 minutes before (3-
28 aminopropyl)triphenylphosphonium bromide (**6**, 3 eq., 0.80 g, 1.66 mmol) and DMAP (0.04 eq.,
29 2.7 μg , 0.02 mmol) were added. The resulting mixture was stirred at room temperature for 5 h,
30 filtered, washed with CH_2Cl_2 , and concentrated to dryness. The crude product was purified by
31 flash chromatography on silica gel using dichloromethane-isopropanol (9.5:0.5) to give an
32 orange powder. Yield: 59%; Rf= 0.45 (dichlorometane-methanol 9:1); mp: 223 °C. ^1H -NMR 400
33 MHz (CDCl_3): δ 8.97 (t, 1H), 7.77-7.73 (m, 10H), 7.62-7.60 (m, 6H), 7.55 (d, 1H), 7.21 (t, 1H),
34 6.78 (d, 1H), 3.92-3.88 (m, 2H), 3.73-3.72 (m, 2H), 1.97 (m, 2H). MS: m/z 439.
35
36
37
38
39
40
41
42
43
44
45
46
47
48
49
50
51

52 **(3-(3-((5,8-Dioxo-5,8-dihydroquinazolin-6-yl)amino)benzamido)propyl)**
53 **triphenylphosphonium bromide (QD359).** A solution of quinazoline-5,8-dione (1.0 eq., 0.04 g,
54
55
56
57
58
59
60

0.25 mmol), cerium (III) chloride heptahydrate ($\text{CeCl}_3 \cdot 7 \text{H}_2\text{O}$, 1.1 eq., 0.102 g, 0.27 mmol) and (3-(3-aminobenzamido)propyl)triphenyl phosphonium bromide (**QD358**, 1.0 eq., 0.130 g, 0.25 mmol) in absolute ethanol (5 mL) was stirred at room temperature for 1.5 h. Then, most of the ethanol was removed under vacuum, and water was added, followed by the extraction with CH_2Cl_2 . The organic layers were washed with water, dried over anhydrous sodium sulphate and concentrated to dryness. The crude product was purified by flash chromatography on silica gel using dichloromethane-methanol (9.4:0.4) to give a red powder. Yield: 30%; $R_f = 0.21$ (dichloromethane-methanol 9:1); mp: 108-110 °C. $^1\text{H-NMR}$ 400 MHz (CDCl_3): δ 9.78 (t, 1H), 9.64 (s, 1H), 9.47 (s, 1H), 8.34 (d, 2H), 8.19 (d, 2H), 7.77-7.73 (m, 10H), 7.64-7.62 (m, 6H), 7.54 (t, 1H), 7.45 (d, 1H), 6.63 (s, 1H), 3.92-3.88 (m, 2H), 3.74-3.73 (m, 2H), 2.05-2.00 (m, 2H). MS: m/z 597.

Biology

Cell Culture. MIA PaCa-2, Panc-1 and BxPC-3 pancreatic cancer cell lines were obtained from the ATCC. Normal pancreatic cells HPDE and HPNE were kindly provided by Dr. Diane Simeone (Translational Oncology Program, University of Michigan, Ann Arbor, MI). Gemcitabine resistant cell line MIA PaCa-2-GR (gemcitabine resistant) was kindly provided by Dr. Sarkar (Department of Pathology, Wayne State University, Detroit, MI) All cell lines were cultured as monolayer and maintained in RPMI1640 supplemented with 10% fetal bovine serum (FBS) in a humidified atmosphere with 5% CO_2 at 37°C. MIA PaCa-2-GR culture was supplemented with 200 nM gemcitabine.

1
2
3 **MTT Assay.** Cytotoxicity of compounds was evaluated with 3-(4,5-dimethylthiazol-2-
4 yl)-2,5-diphenyltetrazolium bromide (MTT) assay. Cells were placed in 96-well plate at 3000-
5 8000 cells/well. After overnight attachment, compounds were added to the wells at sequential
6 dilutions (30 nM – 10 μ M for most cell lines). After 72 h treatment, MTT was added into the
7 media to a final concentration of 300 μ g/mL. Cells were incubated for 3 h at 37°C, and the
8 insoluble formazan converted by viable cells were dissolved in 150 μ L of DMSO. Absorbance at
9 570 nm was read by microplate reader (Molecular devices, Sunnyvale, CA), and inhibition of
10 cell proliferation was calculated using the following formula: Inhibition of cell proliferation (%)
11 = $(1 - OD_{\text{treatment}} / OD_{\text{control}}) \times 100\%$
12
13
14
15
16
17
18
19
20
21
22
23
24
25

26 **ROS Detection Assay.** Cells were detached by 0.05% trypsin-EDTA, neutralized,
27 centrifuged (1200 rpm, 5 min) and resuspended in cell culture media. Suspension were then
28 treated with 20 μ M cell permeable H2DCFDA for 30 min at 37°C. Cells were then centrifuged
29 (1200 rpm, 5min) and washed with cell culture media to remove excess probe. After washing,
30 cells were placed in black-wall 384-well plate at 20,000 cells/well, incubated for 30 min and
31 treated by compounds at designated conditions. Fluorescent signal were then read at 493 nm/523
32 nm on BioTek H1 plate reader for ROS detection.
33
34
35
36
37
38
39
40
41
42
43

44 **Bru-seq Analysis for Nascent RNA Synthesis.** Bru-seq analysis was performed as
45 previously reported³⁶. Briefly, 4×10^6 MIA PaCa-2 cells were placed in 10 cm dishes on Day 1.
46 On Day 2, cells were treated with DMSO, QD232 or QD325 for 4 h. Bromouridine was added
47 into the media to label newly synthesized nascent RNA during the last 30 min of treatment to a
48 final concentration of 2 mM. Cells were then collected in TRIZOL and total RNA was isolated.
49
50
51
52
53
54
55
56
57
58
59
60

1
2
3 Bromouridine-containing RNA was immunocaptured from total RNA, converted into cDNA
4 libraries and deep sequenced at the University of Michigan Sequencing Core. Sequencing reads
5
6 were mapped to the HG19 reference genome. Pre-ranked gene lists were generated for each
7
8 treatment through ranking genes by fold changes in RNA synthesis levels compared with control,
9
10 and analyzed with GSEA (Broad Institute, MA) ^{76, 77}
11
12
13
14
15
16

17 **Western Blotting.** Cells (4×10^5) were cultured in 60 mm tissue dishes and treated with
18
19 QD compounds at designated concentrations. After treatment, cells were lysed with cell lysis
20
21 buffer at 4°C for 30 min and centrifuged (12000 rpm, 10 min, 4°C). Protein concentrations of
22
23 supernatants were measured with BCA assay (Thermo Fisher Scientific). 40 µg protein per
24
25 sample was subjected to SDS-PAGE analysis. Proteins were then electro transferred to methanol
26
27 activated immobilon-FL PVDF membranes (EMD Millipore, Billerica, MA). Membranes were
28
29 blocked with 5% skim milk in TBST buffer and incubated with primary antibodies (anti-NQO1,
30
31 anti-HO-1, anti-CHOP, and anti-GAPDH from Cell Signaling, anti-COXIII, anti-ACTIN and
32
33 anti-GRP78 from Santa Cruz Biotechnology) 1:1000 dilutions overnight at 4°C. Membranes
34
35 were then washed with TBST (10 min x3), incubated with Dylight 800-conjugated secondary
36
37 antibodies (Thermo Fisher Scientific, Rockford, IL) 1:5000 dilutions in 5% milk for 1 h at room
38
39 temperature, and washed with TBST (10 min x2) and TBS (10 min). Fluorescent signal was then
40
41 scanned by Odyssey Imaging Systems (LI-COR Biosciences, Lincoln, NE).
42
43
44
45
46
47
48

49 **Xenograft Studies.** MIA PaCa-2 cells (2.0×10^6) in a 100 µL suspension of RPMI1640
50
51 was injected subcutaneously into dorsal flank of 6-week NOD/SCID mice. Tumor size was
52
53 monitored twice a week through caliper measurement using the following equation: $V = d^2 \times D/2$,
54
55
56
57
58
59
60

1
2
3 where d represents width and D represents length of the tumor. In study 1, mice were randomly
4
5 grouped (n=5 per group) when average tumor size reached 65 mm³. Daily treatment was given at
6
7 five days on two days off cycles. QD325 was given at 5 mg/kg in 100 μL vehicle (5% DMSO,
8
9 60% Propylene glycol, 35% Saline) by intraperitoneal injection. Study was concluded on Day 44
10
11 when average tumor size in the group reached 1200 mm³. Unpaired t test was performed for data
12
13 analysis and $p < 0.05$ was considered significant. For tolerance test, two mice remained on each
14
15 group beyond day 44 and QD325 dose was gradually increased to 20 mg/kg until day 67.
16
17
18 Procedures for study 2 with gemcitabine treatment are detailed in supplemental information.
19
20
21
22
23

24 **Histochemical Analysis.** On necropsy, tumors, hearts, kidneys, livers, lungs, spleens and
25
26 pancreases were collected, fixed in 10% neutral buffered formalin, embedded in paraffin, and
27
28 sectioned. Sections (5 μM) were stained with hematoxylin and eosin to facilitate histologic
29
30 examination. For Ki67 expression level, immunohistochemistry staining was performed on
31
32 sections with Ki67 antibody. Embedding, sectioning and staining of samples were performed by
33
34 ULAM pathology core for animal research at the University of Michigan. Representative images
35
36 were taken on Olympus IX83 microscope with 20X magnification.
37
38
39
40
41

42 ASSOCIATED CONTENT

43 Supporting Information

44
45 The Supporting Information is available free of charge on the ACS Publications website at DOI:
46
47
48 Correlation of cytotoxicity of QD compounds and ROS induction (Figure S2). List of top 30
49
50 canonical pathways affected by QD compound treatments (Figures S3 and S4). List of top 50
51
52 gene sets up regulated by QD compound treatments (Figure S5). List of top 50 gene sets down
53
54
55
56
57
58
59
60

1
2
3 regulated by QD compound treatments (Figure S6). Panels showing QD232 or QD325 treatment
4 that selectively inhibits synthesis of mtDNA transcripts (Figure S7). Elemental analyses for
5 tested compounds (Table S8) (PDF).
6
7
8
9

10 Additional compound data (CSV).
11
12
13
14
15
16

17 **AUTHOR INFORMATION**

18
19 Corresponding authors:
20

21 * N.N. Phone: 734-647-2732. Fax: 734-763-8152. Email: neamati@umich.edu.
22

23 * M.S. Phone: +39 079-228-753. Fax: +39 079-229-559. E-mail: mario.sechi@uniss.it.
24
25
26

27 **Notes**

28 The authors declare the following competing financial interest(s): Certain aspects of the reported
29 compounds are included in patent applications.
30
31
32
33

34 **ACKNOWLEDGMENTS**

35
36 This work was supported by an NIH grant R01 CA188252. MS gratefully acknowledges the
37 Regione Autonoma della Sardegna (within the frame of Legge regionale n. 7/2007), and the
38 Fondazione Banco di Sardegna for its partial support.
39
40
41
42
43
44

45 **ABBREVIATIONS USED**

46
47 Bru-seq, bromouridine labeled RNA sequencing; D-loop, displacement loop; DMAP, 4-
48 dimethylaminopyridine; DIPEA, N,N-diisopropylethylamine; DMF, dimethylformamide; GSEA,
49 Gene Set Enrichment Analysis; HSP, heavy strand promoter; LSP, light strand promoter; ROS,
50 reactive oxygen species; HPLC, high-pressure liquid chromatography; HPDE, human pancreatic
51
52
53
54
55
56
57
58
59
60

1
2
3 ductal epithelial; H2DCFDA, 2',7'-Dichlorodihydrofluorescein diacetate; HBTU (2-(1*H*-
4 benzotriazol-1-yl)-1,1,3,3-tetramethyluronium hexafluorophosphate; IPA, ingenuity pathway
5 analysis; IC50, half-maximum inhibitory concentration; MTT, 3-(4,5-dimethylthiazol-2-yl)-2,5-
6 diphenyltetrazolium bromide; mtDNA, mitochondrial DNA; NAC, N-acetyl-cysteine; PBS,
7 phosphate-buffered saline; PDAC, pancreatic ductal adenocarcinoma; QDs, quinazolinediones;
8 UPR, unfolded protein response.
9
10
11
12
13
14
15
16
17
18
19
20
21
22
23
24
25
26
27
28
29
30
31
32
33
34
35
36
37
38
39
40
41
42
43
44
45
46
47
48
49
50
51
52
53
54
55
56
57
58
59
60

REFERENCES

1. Siegel, R. L.; Miller, K. D.; Jemal, A. Cancer statistics, 2017. *CA Cancer J Clin* **2017**, *67*, 7-30.
2. Sohal, D. P.; Mangu, P. B.; Khorana, A. A.; Shah, M. A.; Philip, P. A.; O'Reilly, E. M.; Uronis, H. E.; Ramanathan, R. K.; Crane, C. H.; Engebretson, A.; Ruggiero, J. T.; Copur, M. S.; Lau, M.; Urba, S.; Laheru, D. Metastatic pancreatic cancer: American Society of Clinical Oncology clinical practice guideline. *J Clin Oncol* **2016**, *34*, 2784-2796.
3. Ryan, D. P.; Hong, T. S.; Bardeesy, N. Pancreatic adenocarcinoma. *N Engl J Med* **2014**, *371*, 1039-1049.
4. Von Hoff, D. D.; Ervin, T.; Arena, F. P.; Chiorean, E. G.; Infante, J.; Moore, M.; Seay, T.; Tjulandin, S. A.; Ma, W. W.; Saleh, M. N.; Harris, M.; Reni, M.; Dowden, S.; Laheru, D.; Bahary, N.; Ramanathan, R. K.; Tabernero, J.; Hidalgo, M.; Goldstein, D.; Van Cutsem, E.; Wei, X.; Iglesias, J.; Renschler, M. F. Increased survival in pancreatic cancer with nab-paclitaxel plus gemcitabine. *N Engl J Med* **2013**, *369*, 1691-1703.
5. Conroy, T.; Desseigne, F.; Ychou, M.; Bouche, O.; Guimbaud, R.; Becouarn, Y.; Adenis, A.; Raoul, J. L.; Gourgou-Bourgade, S.; de la Fouchardiere, C.; Bennouna, J.; Bachet, J. B.; Khemissa-Akouz, F.; Pere-Verge, D.; Delbaldo, C.; Assenat, E.; Chauffert, B.; Michel, P.; Montoto-Grillot, C.; Ducreux, M.; Groupe Tumeurs Digestives of, U.; Intergroup, P. FOLFIRINOX versus gemcitabine for metastatic pancreatic cancer. *N Engl J Med* **2011**, *364*, 1817-1825.
6. Kamisawa, T.; Wood, L. D.; Itoi, T.; Takaori, K. Pancreatic cancer. *Lancet* **2016**, *388*, 73-85.
7. Suker, M.; Beumer, B. R.; Sadot, E.; Marthey, L.; Faris, J. E.; Mellon, E. A.; El-Rayes, B. F.; Wang-Gillam, A.; Lacy, J.; Hosein, P. J.; Moorcraft, S. Y.; Conroy, T.; Hohla, F.; Allen, P.;

- 1
2
3 Taieb, J.; Hong, T. S.; Shridhar, R.; Chau, I.; van Eijck, C. H.; Koerkamp, B. G.
4
5 FOLFIRINOX for locally advanced pancreatic cancer: a systematic review and patient-level
6
7 meta-analysis. *Lancet Oncol* **2016**, *17*, 801-810.
8
9
- 10 8. Conroy, T.; Bachet, J. B.; Ayav, A.; Huguet, F.; Lambert, A.; Caramella, C.; Marechal, R.;
11
12 Van Laethem, J. L.; Ducreux, M. Current standards and new innovative approaches for
13
14 treatment of pancreatic cancer. *Eur J Cancer* **2016**, *57*, 10-22.
15
16
- 17 9. Fogel, E. L.; Shahda, S.; Sandrasegaran, K.; DeWitt, J.; Easler, J. J.; Agarwal, D. M.;
18
19 Eagleson, M.; Zyromski, N. J.; House, M. G.; Ellsworth, S.; El Hajj, I.; O'Neil, B. H.;
20
21 Nakeeb, A.; Sherman, S. A multidisciplinary approach to pancreas cancer in 2016: A review.
22
23 *Am J Gastroenterol* **2017**, *112*, 537-554.
24
25
- 26 10. Falasca, M.; Kim, M.; Casari, I. Pancreatic cancer: Current research and future directions.
27
28 *Biochim Biophys Acta* **2016**, *1865*, 123-132.
29
30
- 31 11. Mukherjee, I.; Powell, B.; Parianos, M.; Downs, D.; Ross, S. B. Available technologies and
32
33 clinical applications of targeted chemotherapy in pancreatic cancer. *Cancer Genet* **2016**, *209*,
34
35 582-591.
36
37
- 38 12. Martinez-Useros, J.; Li, W.; Cabeza-Morales, M.; Garcia-Foncillas, J. Oxidative stress: A
39
40 new target for pancreatic cancer prognosis and treatment. *J Clin Med* **2017**, *6*, 29.
41
42
- 43 13. Trachootham, D.; Alexandre, J.; Huang, P. Targeting cancer cells by ROS-mediated
44
45 mechanisms: a radical therapeutic approach? *Nat Rev Drug Discov* **2009**, *8*, 579-591.
46
47
- 48 14. Moloney, J. N.; Cotter, T. G. ROS signalling in the biology of cancer. *Semin Cell Dev Biol*
49
50 **2017**. Doi: 10.1016/j.semcdb.2017.05.023. Published Online: June 3, 2017.
51
52
- 53 15. Idelchik, M.; Begley, U.; Begley, T. J.; Melendez, J. A. Mitochondrial ROS control of cancer.
54
55 *Semin Cancer Biol* **2017**, *47*, 57-66.
56
57
58
59
60

- 1
2
3 16. Dharmaraja, A. T. Role of reactive oxygen species (ROS) in therapeutics and drug resistance
4 in cancer and bacteria. *J Med Chem* **2017**, *60*, 3221-3240.
5
6
7
8 17. Panieri, E.; Santoro, M. M. ROS homeostasis and metabolism: a dangerous liason in cancer
9 cells. *Cell Death Dis* **2016**, *7*, e2253.
10
11
12 18. Diebold, L.; Chandel, N. S. Mitochondrial ROS regulation of proliferating cells. *Free Radic*
13 *Biol Med* **2016**, *100*, 86-93.
14
15
16
17 19. Li, X.; Fang, P.; Mai, J.; Choi, E. T.; Wang, H.; Yang, X. F. Targeting mitochondrial reactive
18 oxygen species as novel therapy for inflammatory diseases and cancers. *J Hematol Oncol*
19 **2013**, *6*, 19.
20
21
22
23
24 20. Chio, I. I. C.; Tuveson, D. A. ROS in cancer: The burning question. *Trends Mol Med* **2017**,
25 *23*, 411-429.
26
27
28
29 21. Fruehauf, J. P.; Meyskens, F. L., Jr. Reactive oxygen species: a breath of life or death? *Clin*
30 *Cancer Res* **2007**, *13*, 789-794.
31
32
33 22. DeNicola, G. M.; Karreth, F. A.; Humpton, T. J.; Gopinathan, A.; Wei, C.; Frese, K.; Mangal,
34 D.; Yu, K. H.; Yeo, C. J.; Calhoun, E. S.; Scrimieri, F.; Winter, J. M.; Hruban, R. H.;
35 Iacobuzio-Donahue, C.; Kern, S. E.; Blair, I. A.; Tuveson, D. A. Oncogene-induced Nrf2
36 transcription promotes ROS detoxification and tumorigenesis. *Nature* **2011**, *475*, 106-109.
37
38
39
40
41
42 23. Kong, B.; Qia, C.; Erkan, M.; Kleeff, J.; Michalski, C. W. Overview on how oncogenic Kras
43 promotes pancreatic carcinogenesis by inducing low intracellular ROS levels. *Front Physiol*
44 **2013**, *4*, 246.
45
46
47
48
49 24. Storz, P. KRas, ROS and the initiation of pancreatic cancer. *Small GTPases* **2017**, *8*, 38-42.
50
51
52 25. Zhang, L.; Li, J.; Ma, J.; Chen, X.; Chen, K.; Jiang, Z.; Zong, L.; Yu, S.; Li, X.; Xu, Q.; Lei,
53 J.; Duan, W.; Li, W.; Shan, T.; Ma, Q.; Shen, X. The relevance of Nrf2 pathway and
54
55
56
57
58
59
60

- 1
2
3 autophagy in pancreatic cancer cells upon stimulation of reactive oxygen species. *Oxid Med*
4 *Cell Longev* **2016**, *2016*, 3897250.
- 5
6
7
8 26. Pelicano, H.; Carney, D.; Huang, P. ROS stress in cancer cells and therapeutic implications.
9
10 *Drug Resist Updat* **2004**, *7*, 97-110.
- 11
12 27. Sabharwal, S. S.; Schumacker, P. T. Mitochondrial ROS in cancer: initiators, amplifiers or an
13
14 Achilles' heel? *Nat Rev Cancer* **2014**, *14*, 709-721.
- 15
16
17 28. Durand, N.; Storz, P. Targeting reactive oxygen species in development and progression of
18
19 pancreatic cancer. *Expert Rev Anticancer Ther* **2017**, *17*, 19-31.
- 20
21
22 29. Pathania, D.; Kuang, Y.; Sechi, M.; Neamati, N. Mechanisms underlying the cytotoxicity of
23
24 a novel quinazolidione-based redox modulator, QD232, in pancreatic cancer cells. *Br J*
25
26 *Pharmacol* **2015**, *172*, 50-63.
- 27
28
29 30. Pathania, D.; Sechi, M.; Palomba, M.; Sanna, V.; Berrettini, F.; Sias, A.; Taheri, L.; Neamati,
30
31 N. Design and discovery of novel quinazolidione-based redox modulators as therapies for
32
33 pancreatic cancer. *Biochim Biophys Acta* **2014**, *1840*, 332-343.
- 34
35
36 31. Madak, J. T.; Neamati, N. Membrane permeable lipophilic cations as mitochondrial directing
37
38 groups. *Curr Top Med Chem* **2015**, *15*, 745-766.
- 39
40
41 32. Millard, M.; Gallagher, J. D.; Olenyuk, B. Z.; Neamati, N. A selective mitochondrial-targeted
42
43 chlorambucil with remarkable cytotoxicity in breast and pancreatic cancers. *J Med Chem*
44
45 **2013**, *56*, 9170-9179.
- 46
47 33. Madak, J. T.; Cuthbertson, C. R.; Chen, W.; Showalter, H. D.; Neamati, N. Design, synthesis,
48
49 and characterization of brequinar conjugates as probes to study DHODH inhibition.
50
51 *Chemistry Eur J* **2017**, *23*, 13875-13878.
- 52
53
54
55
56
57
58
59
60

- 1
2
3 34. Ali, S.; Almhanna, K.; Chen, W.; Philip, P. A.; Sarkar, F. H. Differentially expressed
4 miRNAs in the plasma may provide a molecular signature for aggressive pancreatic cancer.
5
6
7
8 *Am J Transl Res* **2010**, *3*, 28-47.
9
- 10 35. Ouyang, H.; Mou, L.; Luk, C.; Liu, N.; Karaskova, J.; Squire, J.; Tsao, M. S. Immortal
11 human pancreatic duct epithelial cell lines with near normal genotype and phenotype. *Am J*
12
13 *Pathol* **2000**, *157*, 1623-1631.
14
15
16
- 17 36. Paulsen, M. T.; Veloso, A.; Prasad, J.; Bedi, K.; Ljungman, E. A.; Magnuson, B.; Wilson, T.
18
19 E.; Ljungman, M. Use of Bru-Seq and BruChase-Seq for genome-wide assessment of the
20
21
22 synthesis and stability of RNA. *Methods* **2014**, *67*, 45-54.
23
- 24 37. Paulsen, M. T.; Veloso, A.; Prasad, J.; Bedi, K.; Ljungman, E. A.; Tsan, Y. C.; Chang, C.
25
26 W.; Tarrier, B.; Washburn, J. G.; Lyons, R.; Robinson, D. R.; Kumar-Sinha, C.; Wilson, T.
27
28 E.; Ljungman, M. Coordinated regulation of synthesis and stability of RNA during the acute
29
30
31 TNF-induced proinflammatory response. *Proc Natl Acad Sci U S A* **2013**, *110*, 2240-2245.
32
- 33 38. Jaiswal, A. K. Nrf2 signaling in coordinated activation of antioxidant gene expression. *Free*
34
35 *Radic Biol Med* **2004**, *36*, 1199-1207.
36
- 37 39. Dinkova-Kostova, A. T.; Holtzclaw, W. D.; Cole, R. N.; Itoh, K.; Wakabayashi, N.; Katoh,
38
39 Y.; Yamamoto, M.; Talalay, P. Direct evidence that sulfhydryl groups of Keap1 are the
40
41
42 sensors regulating induction of phase 2 enzymes that protect against carcinogens and
43
44
45 oxidants. *Proc Natl Acad Sci U S A* **2002**, *99*, 11908-11913.
46
- 47 40. Zhang, D. D.; Hannink, M. Distinct cysteine residues in Keap1 are required for Keap1-
48
49
50 dependent ubiquitination of Nrf2 and for stabilization of Nrf2 by chemopreventive agents
51
52
53 and oxidative stress. *Mol Cell Biol* **2003**, *23*, 8137-8151.
54
55
56
57
58
59
60

- 1
2
3
4
5
6
7
8
9
10
11
12
13
14
15
16
17
18
19
20
21
22
23
24
25
26
27
28
29
30
31
32
33
34
35
36
37
38
39
40
41
42
43
44
45
46
47
48
49
50
51
52
53
54
55
56
57
58
59
60
41. Alam, J.; Stewart, D.; Touchard, C.; Boinapally, S.; Choi, A. M.; Cook, J. L. Nrf2, a Cap'n'Collar transcription factor, regulates induction of the heme oxygenase-1 gene. *J Biol Chem* **1999**, *274*, 26071-26078.
42. Nioi, P.; McMahon, M.; Itoh, K.; Yamamoto, M.; Hayes, J. D. Identification of a novel Nrf2-regulated antioxidant response element (ARE) in the mouse NAD(P)H:quinone oxidoreductase 1 gene: reassessment of the ARE consensus sequence. *Biochem J* **2003**, *374*, 337-348.
43. Ross, D.; Kepa, J. K.; Winski, S. L.; Beall, H. D.; Anwar, A.; Siegel, D. NAD(P)H:quinone oxidoreductase 1 (NQO1): chemoprotection, bioactivation, gene regulation and genetic polymorphisms. *Chem Biol Interact* **2000**, *129*, 77-97.
44. Dinkova-Kostova, A. T.; Talalay, P. Persuasive evidence that quinone reductase type 1 (DT diaphorase) protects cells against the toxicity of electrophiles and reactive forms of oxygen. *Free Radic Biol Med* **2000**, *29*, 231-240.
45. Choi, A. M.; Alam, J. Heme oxygenase-1: function, regulation, and implication of a novel stress-inducible protein in oxidant-induced lung injury. *Am J Respir Cell Mol Biol* **1996**, *15*, 9-19.
46. Shamu, C. E.; Walter, P. Oligomerization and phosphorylation of the Ire1p kinase during intracellular signaling from the endoplasmic reticulum to the nucleus. *EMBO J* **1996**, *15*, 3028-3039.
47. Harding, H. P.; Zhang, Y.; Bertolotti, A.; Zeng, H.; Ron, D. Perk is essential for translational regulation and cell survival during the unfolded protein response. *Mol Cell* **2000**, *5*, 897-904.

- 1
2
3 48. Haze, K.; Yoshida, H.; Yanagi, H.; Yura, T.; Mori, K. Mammalian transcription factor ATF6
4 is synthesized as a transmembrane protein and activated by proteolysis in response to
5 endoplasmic reticulum stress. *Mol Biol Cell* **1999**, *10*, 3787-3799.
6
7
8
9
10 49. Hetz, C. The unfolded protein response: controlling cell fate decisions under ER stress and
11 beyond. *Nat Rev Mol Cell Biol* **2012**, *13*, 89-102.
12
13
14 50. Kim, R.; Emi, M.; Tanabe, K.; Murakami, S. Role of the unfolded protein response in cell
15 death. *Apoptosis* **2006**, *11*, 5-13.
16
17
18 51. Verfaillie, T.; Garg, A. D.; Agostinis, P. Targeting ER stress induced apoptosis and
19 inflammation in cancer. *Cancer Lett* **2013**, *332*, 249-264.
20
21
22 52. Nishitoh, H. CHOP is a multifunctional transcription factor in the ER stress response. *J*
23 *Biochem* **2012**, *151*, 217-219.
24
25
26 53. Oyadomari, S.; Mori, M. Roles of CHOP/GADD153 in endoplasmic reticulum stress. *Cell*
27 *Death Differ* **2004**, *11*, 381-389.
28
29
30 54. Ghosh, A. P.; Klocke, B. J.; Ballestas, M. E.; Roth, K. A. CHOP potentially co-operates with
31 FOXO3a in neuronal cells to regulate PUMA and BIM expression in response to ER stress.
32 *PloS one* **2012**, *7*, e39586.
33
34
35 55. Jutooru, I.; Chadalapaka, G.; Lei, P.; Safe, S. Inhibition of NFkappaB and pancreatic cancer
36 cell and tumor growth by curcumin is dependent on specificity protein down-regulation. *J*
37 *Biol Chem* **2010**, *285*, 25332-25344.
38
39
40 56. Kasiappan, R.; Jutooru, I.; Karki, K.; Hedrick, E.; Safe, S. Benzyl isothiocyanate (BITC)
41 induces reactive oxygen species-dependent repression of STAT3 protein by down-regulation
42 of specificity proteins in pancreatic cancer. *J Biol Chem* **2016**, *291*, 27122-27133.
43
44
45
46
47
48
49
50
51
52
53
54
55
56
57
58
59
60

- 1
2
3 57. Jutooru, I.; Guthrie, A. S.; Chadalapaka, G.; Pathi, S.; Kim, K.; Burghardt, R.; Jin, U. H.;
4
5 Safe, S. Mechanism of action of phenethylisothiocyanate and other reactive oxygen species-
6
7 inducing anticancer agents. *Mol Cell Biol* **2014**, *34*, 2382-2395.
8
9
10 58. Guleng, G.; Lovig, T.; Meling, G. I.; Andersen, S. N.; Rognum, T. O. Mitochondrial
11
12 microsatellite instability in colorectal carcinomas--frequency and association with nuclear
13
14 microsatellite instability. *Cancer Lett* **2005**, *219*, 97-103.
15
16
17 59. Kabekkodu, S. P.; Bhat, S.; Mascarenhas, R.; Mallya, S.; Bhat, M.; Pandey, D.; Kushtagi, P.;
18
19 Thangaraj, K.; Gopinath, P. M.; Satyamoorthy, K. Mitochondrial DNA variation analysis in
20
21 cervical cancer. *Mitochondrion* **2014**, *16*, 73-82.
22
23
24 60. Suzuki, M.; Toyooka, S.; Miyajima, K.; Iizasa, T.; Fujisawa, T.; Bekele, N. B.; Gazdar, A. F.
25
26 Alterations in the mitochondrial displacement loop in lung cancers. *Clin Cancer Res* **2003**, *9*,
27
28 5636-5641.
29
30
31 61. Wheelhouse, N. M.; Lai, P. B.; Wigmore, S. J.; Ross, J. A.; Harrison, D. J. Mitochondrial D-
32
33 loop mutations and deletion profiles of cancerous and noncancerous liver tissue in hepatitis B
34
35 virus-infected liver. *Br J Cancer* **2005**, *92*, 1268-1272.
36
37
38 62. Lievre, A.; Chapusot, C.; Bouvier, A. M.; Zinzindohoue, F.; Piard, F.; Roignot, P.; Arnould,
39
40 L.; Beaune, P.; Faivre, J.; Laurent-Puig, P. Clinical value of mitochondrial mutations in
41
42 colorectal cancer. *J Clin Oncol* **2005**, *23*, 3517-3525.
43
44
45 63. Ye, K.; Lu, J.; Ma, F.; Keinan, A.; Gu, Z. Extensive pathogenicity of mitochondrial
46
47 heteroplasmy in healthy human individuals. *Proc Natl Acad Sci U S A* **2014**, *111*, 10654-
48
49 10659.
50
51
52 64. Na, H. K.; Surh, Y. J. Oncogenic potential of Nrf2 and its principal target protein heme
53
54 oxygenase-1. *Free Radic Biol Med* **2014**, *67*, 353-365.
55
56
57
58
59
60

- 1
2
3 65. Moon, E. J.; Giaccia, A. Dual roles of NRF2 in tumor prevention and progression: Possible
4 implications in cancer treatment. *Free Radic Biol Med* **2014**, *79*, 292-299.
5
6
7
8 66. Hayes, J. D.; McMahon, M. NRF2 and KEAP1 mutations: permanent activation of an
9 adaptive response in cancer. *Trends Biochem Sci* **2009**, *34*, 176-188.
10
11
12 67. Lister, A.; Nedjadi, T.; Kitteringham, N. R.; Campbell, F.; Costello, E.; Lloyd, B.; Copple, I.
13 M.; Williams, S.; Owen, A.; Neoptolemos, J. P.; Goldring, C. E.; Park, B. K. Nrf2 is
14 overexpressed in pancreatic cancer: implications for cell proliferation and therapy. *Mol*
15 *Cancer* **2011**, *10*, 37.
16
17
18
19
20
21 68. Arlt, A.; Sebens, S.; Krebs, S.; Geismann, C.; Grossmann, M.; Kruse, M. L.; Schreiber, S.;
22 Schafer, H. Inhibition of the Nrf2 transcription factor by the alkaloid trigonelline renders
23 pancreatic cancer cells more susceptible to apoptosis through decreased proteasomal gene
24 expression and proteasome activity. *Oncogene* **2013**, *32*, 4825-4835.
25
26
27
28
29
30 69. Dhillon, H.; Chikara, S.; Reindl, K. M. Piperlongumine induces pancreatic cancer cell death
31 by enhancing reactive oxygen species and DNA damage. *Toxicol Rep* **2014**, *1*, 309-318.
32
33
34
35 70. Dorr, R. T.; Raymond, M. A.; Landowski, T. H.; Roman, N. O.; Fukushima, S. Induction of
36 apoptosis and cell cycle arrest by imexon in human pancreatic cancer cell lines. *Int J*
37 *Gastrointest Cancer* **2005**, *36*, 15-28.
38
39
40
41
42 71. Cohen, S. J.; Zalupski, M. M.; Modiano, M. R.; Conkling, P.; Patt, Y. Z.; Davis, P.; Dorr, R.
43 T.; Boytim, M. L.; Hersh, E. M. A phase I study of imexon plus gemcitabine as first-line
44 therapy for advanced pancreatic cancer. *Cancer Chemother Pharmacol* **2010**, *66*, 287-294.
45
46
47
48
49 72. Malhotra, J. D.; Kaufman, R. J. Endoplasmic reticulum stress and oxidative stress: a vicious
50 cycle or a double-edged sword? *Antioxid Redox Signal* **2007**, *9*, 2277-2293.
51
52
53
54
55
56
57
58
59
60

- 1
2
3 73. Falkenberg, M.; Larsson, N. G.; Gustafsson, C. M. DNA replication and transcription in
4 mammalian mitochondria. *Annu Rev Biochem* **2007**, *76*, 679-699.
5
6
7
8 74. Montoya, J.; Gaines, G. L.; Attardi, G. The pattern of transcription of the human
9 mitochondrial rRNA genes reveals two overlapping transcription units. *Cell* **1983**, *34*, 151-9.
10
11
12 75. Ojala, D.; Montoya, J.; Attardi, G. tRNA punctuation model of RNA processing in human
13 mitochondria. *Nature* **1981**, *290*, 470-474.
14
15
16
17 76. Subramanian, A.; Tamayo, P.; Mootha, V. K.; Mukherjee, S.; Ebert, B. L.; Gillette, M. A.;
18 Paulovich, A.; Pomeroy, S. L.; Golub, T. R.; Lander, E. S.; Mesirov, J. P. Gene set
19 enrichment analysis: a knowledge-based approach for interpreting genome-wide expression
20 profiles. *Proc Natl Acad Sci U S A* **2005**, *102*, 15545-15550.
21
22
23
24
25
26 77. Mootha, V. K.; Lindgren, C. M.; Eriksson, K. F.; Subramanian, A.; Sihag, S.; Lehar, J.;
27 Puigserver, P.; Carlsson, E.; Ridderstrale, M.; Laurila, E.; Houstis, N.; Daly, M. J.; Patterson,
28 N.; Mesirov, J. P.; Golub, T. R.; Tamayo, P.; Spiegelman, B.; Lander, E. S.; Hirschhorn, J.
29 N.; Altshuler, D.; Groop, L. C. PGC-1alpha-responsive genes involved in oxidative
30 phosphorylation are coordinately downregulated in human diabetes. *Nat Genet* **2003**, *34*,
31 267-273.
32
33
34
35
36
37
38
39
40
41
42
43
44
45
46
47
48
49
50
51
52
53
54
55
56
57
58
59
60

Figure legends

Figure 1. Cytotoxicity of the QD compounds is reduced by NAC in MIA PaCa-2 cells. A) The parental compound QD232 induces ROS accumulation in a dose and time-dependent manner. The new analogues QD325 and QD326 induced a stronger and more rapid ROS accumulation in MIA PaCa-2 cells than the parental QD232 compound. Compounds were tested at 10, 3.3 or 1.1 μM . DMSO was used as a negative control to determine the basal signal of the assay (DMSO). Cells without preloaded H2DCFDA were treated with compounds at 10 μM at the same conditions to determine the endogenous fluorescence of the compounds (no stain). Data points represent mean \pm SD from duplicates. Graphs are representatives of three independent experiments. B) ROS induction by QD232, 325 and 326 was inhibited by NAC pretreatment (5 mM for 30 min). Data points represent mean \pm SD from duplicates. Graphs are representatives of three independent experiments. C) Presence of NAC at 5 mM decreased the cytotoxicity of the QD232, QD325 and QD326 compounds. Cytotoxicity was determined by the MTT assay after a 72 h treatment. Data points represent mean \pm SD from three independent experiments.

Figure 2. The QD compounds induce oxidative stress and the unfolded protein response. A) Top 15 canonical pathways induced by QD232 or QD325 treatment as revealed by IPA analysis of Bru-seq data. MIA PaCa-2 cells were treated with QD232 (at 1, 2 or 3 times IC_{50}) or QD325 (at 1, 2 or 5 times IC_{50}) for 4 h. Nascent RNA was labeled with 2 mM bromouridine during the last 30 min of treatment, immunocaptured, converted to cDNA libraries and deep sequenced. B) Transcription of oxidative stress responsive genes *NQO1* and *HMOX1* was upregulated by QD232 or QD325 treatment in MIA PaCa-2 cells in a dose-dependent manner. C) Transcription

1
2
3 of unfolded protein response target genes *DDIT3* and *HSPA5* was upregulated by QD232 or
4 QD325 treatment in MIA PaCa-2 cells.
5
6
7
8
9

10 **Figure 3.** The QD compounds induce protein expression of target genes for oxidative stress and
11 unfolded protein response. Expression levels of oxidative stress responsive proteins NQO1, HO-
12 1 and unfolded protein response target proteins CHOP and GRP78 were regulated to different
13 extents by QD232 or QD325 treatment time dependently in A) MIA PaCa-2, B) Panc-1 and C)
14 BxPC-3 cells. Protein levels were quantified by ImageJ and normalized to respective loading
15 controls. Data on quantification plots represent mean \pm SD from three independent experiments.
16
17 P values were calculated using student's t-test. *, $p < 0.05$; **, $p < 0.01$, ***, $p < 0.001$.
18
19
20
21
22
23
24
25
26
27

28 **Figure 4.** The QD compounds show selective inhibition of transcription from the mitochondrial
29 genome. A) Nascent mitochondrial RNA synthesis was inhibited following a 4-hour treatment
30 with QD232 (at 6.9 μ M) or QD325 (at 5.0 μ M) in MIA PaCa-2 cells. Top forward arrows
31 represent transcripts from the heavy strand. While the shorter arrow represents the shorter rRNA
32 transcript regulated by the HSP1 promoter, the longer arrow represents transcript regulated by
33 the HSP2 promoter that covers the full length of the heavy strand of the mitochondrial genome.
34 Bottom reverse arrow represents the light strand transcript regulated by the LSP promoter.
35 Transcription signals from DMSO-treated control cells are shown in yellow while transcription
36 signals from the QD232-treated cells are shown in blue, and signals from the QD325-treated
37 cells are shown in red. The full-length transcripts from both heavy and light strands are further
38 processed into functional tRNA, rRNA and mRNA molecules, whose corresponding genes are
39 shown at the bottom of the panel. B) Protein (COXIII) expression levels of the mitochondrial
40
41
42
43
44
45
46
47
48
49
50
51
52
53
54
55
56
57
58
59
60

1
2
3 gene *COIII* were decreased by treatment of the QD compounds in MIA PaCa-2 cells. Protein
4 levels were quantified by ImageJ and normalized to respective loading controls. Data on
5 quantification plots represent mean \pm SD from three independent experiments. P-values were
6 calculated using student's t-test. *, $p < 0.05$; **, $p < 0.01$.
7
8
9
10
11
12
13

14 **Figure 5.** QD325 inhibits tumor growth of MIA PaCa-2 xenograft without systemic toxicity. A)
15 MIA PaCa-2 engrafted NOD/SCID mice were randomized into vehicle control (n=5) or QD325
16 treatment (n=5) group when tumor size reached 65 mm³. QD325 was given at 5 mg/kg five times
17 a week until day 44. B) Body weight of engrafted mice was not affected by QD325 treatment at
18 5 mg/kg five times a week until day 44. Data points represent mean \pm SEM. C) Representative
19 micrographs of hematoxylin and eosin (H&E)-stained organ sections. Images were taken with an
20 Olympus IX83 inverted microscope at 20X magnification. Histopathology inspection showed no
21 major microscopic changes in major organs after QD325 treatment at 5 mg/kg five times a week
22 until day 44. D) Representative immunohistochemistry images for Ki67 staining of MIA PaCa-2
23 xenograft sections. QD325 decreased Ki67 index (percentage of Ki67 positive cells in the field)
24 of treated tumors. Data represents mean \pm SD (n=9, 3 tumors from each group, 3 images of each
25 tumor section). P-values were calculated using student's t-test. E) NQO1, HO-1, CHOP, GRP78
26 protein levels in vehicle or QD325-treated MIA PaCa-2 xenografts.
27
28
29
30
31
32
33
34
35
36
37
38
39
40
41
42
43
44
45
46

47 **Figure 6.** QD325 inhibits tumor growth of MIA PaCa-2 xenograft. A) QD325 treatment at 5
48 mg/kg inhibits growth of MIA PaCa-2 xenograft in NOD/SCID mice. MIA PaCa-2 engrafted
49 mice were randomized into vehicle control (n=5) or QD325 treatment (n=5) group when tumor
50 size reached 65 mm³. QD325 was given at 5 mg/kg five times a week until day 44. Three mice
51
52
53
54
55
56
57
58
59
60

1
2
3 from each group were euthanized for tissue analysis. Two mice remained in each group after day
4 44 and QD325 dose was increased from 5 mg/kg to 20 mg/kg until day 67. B) Body weight of
5 engrafted mice was not affected by QD325 treatment from 5 to 20 mg/kg. Error bars indicate
6 mean \pm SEM. C) Gemcitabine treatment at 15 mg/kg inhibits growth of MIA PaCa-2 xenograft
7 in NOD/SCID mice. MIA PaCa-2 engrafted mice were randomized into vehicle control (n=4),
8 gemcitabine treatment 1 (n=3), gemcitabine treatment 2 (n=4) groups when tumor size reached
9 75mm³. In treatment 1, gemcitabine was given at 15 mg/kg once a week for 48 days; in treatment
10 2, gemcitabine was given at 15 mg/kg twice a week for 15 days. Data points represent mean \pm
11 SEM. D) Body weight of engrafted mice is not affected by gemcitabine treatment in either
12 dosing frequency. E) QD325 treatment at 5 mg/kg inhibits growth of MIA PaCa-2 xenograft in
13 NOD/SCID mice. MIA PaCa-2 engrafted mice were randomized into vehicle control (n=4),
14 gemcitabine treatment (n=3), QD325 treatment (n=3) and combination treatment groups (n=3)
15 when tumor size reached 75mm³. QD325 was given at 5 mg/kg five times a week and
16 gemcitabine was given at 15 mg/kg once a week. Data points represent mean \pm SEM. F) Body
17 weight of engrafted mice was not affected by gemcitabine or QD325 treatment.
18
19
20
21
22
23
24
25
26
27
28
29
30
31
32
33
34
35
36
37
38
39
40
41
42
43
44
45
46
47
48
49
50
51
52
53
54
55
56
57
58
59
60

Chart 1. Select examples of drugs containing quinone or a Michael acceptor that are FDA approved or under clinical investigations for various diseases

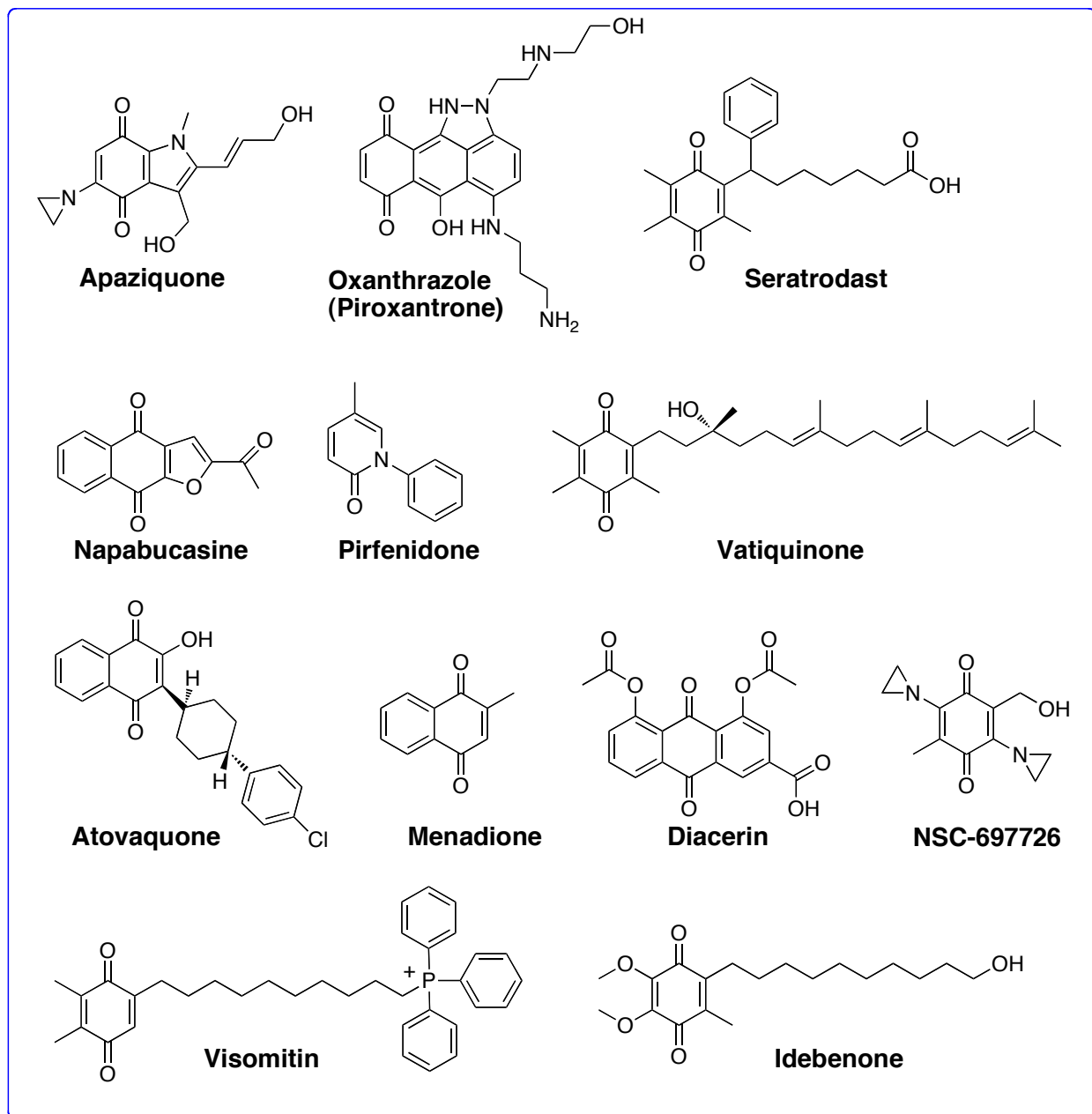
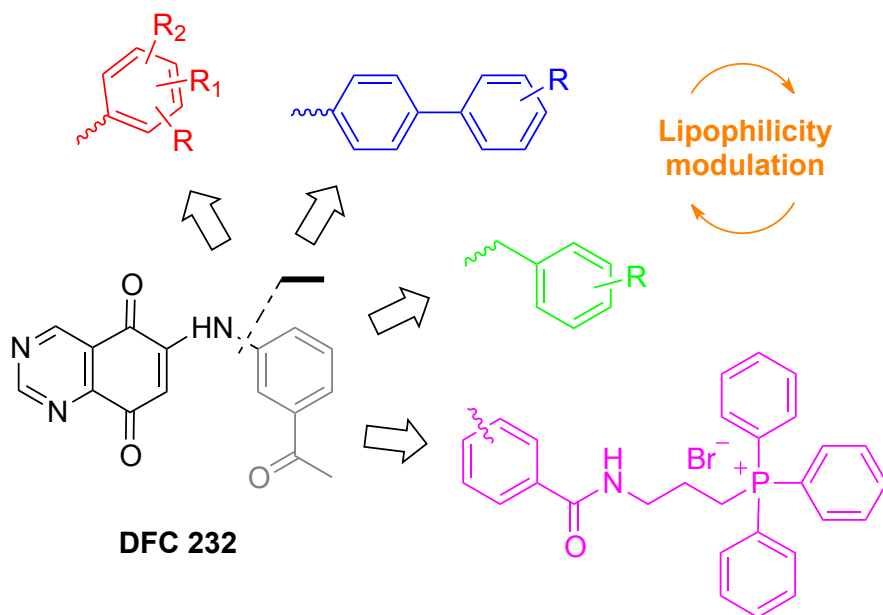
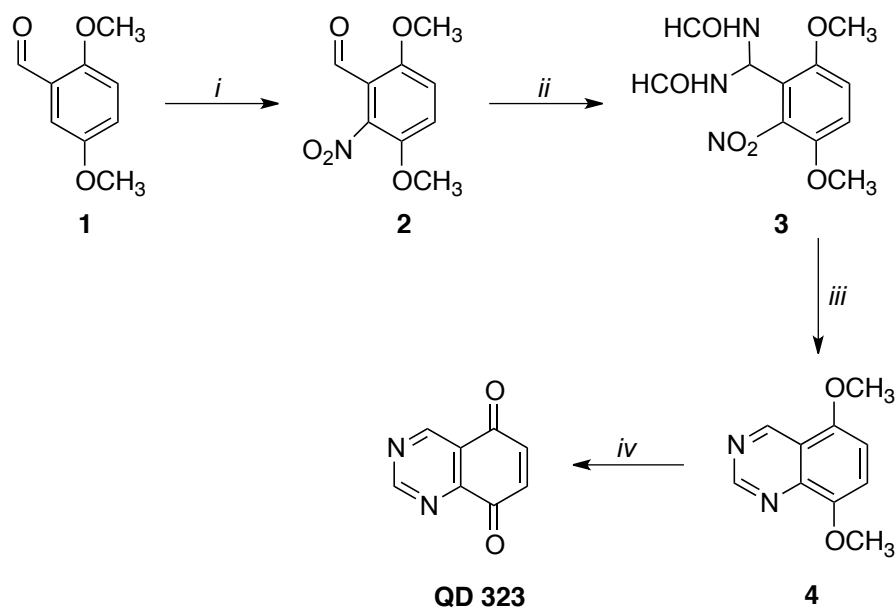


Chart 2. Structure of Lead Compound QD 232 and Design of Title Compounds.



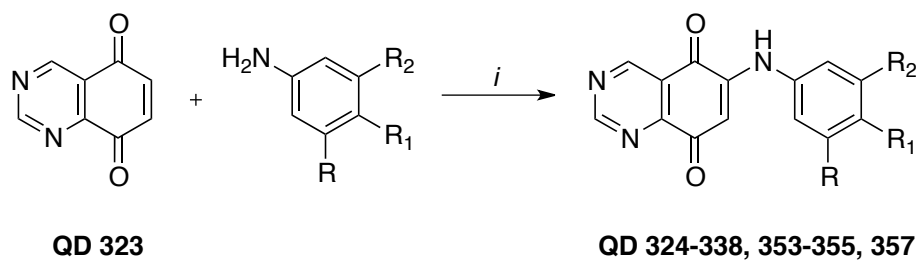
$R, R_1, R_2 = H, Me, Et, F, OCH_3, OCF_3, OPh, COOMe, COOEt, CH_2OH, NH_2, CONH_2, SO_2NH_2, B(OH)_2$

Scheme 1.^a Synthetic route for the preparation of the key intermediate **QD 323**.

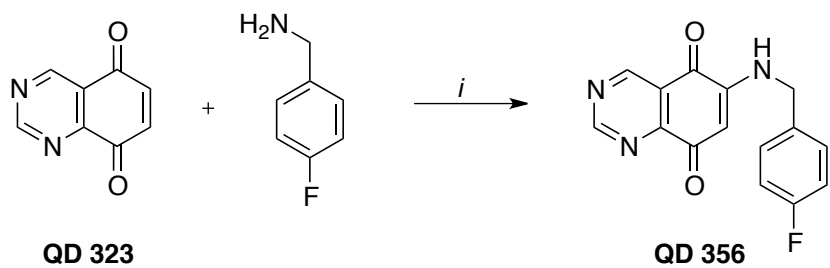


^a**Reagents and conditions:** (i) conc. HNO₃, (CH₃CO)₂O, 0 °C, 1.5 h; (ii) H₂NCHO, HCl_(g) from 40 to 80 °C, 1h; (iii) glacial CH₃COOH, Zn, 0 °C for 2 h, r.t. for 4 h; (iv) (NH₄)₂Ce(NO₃)₆, CH₃CN/H₂O, 0 °C, 20 min.

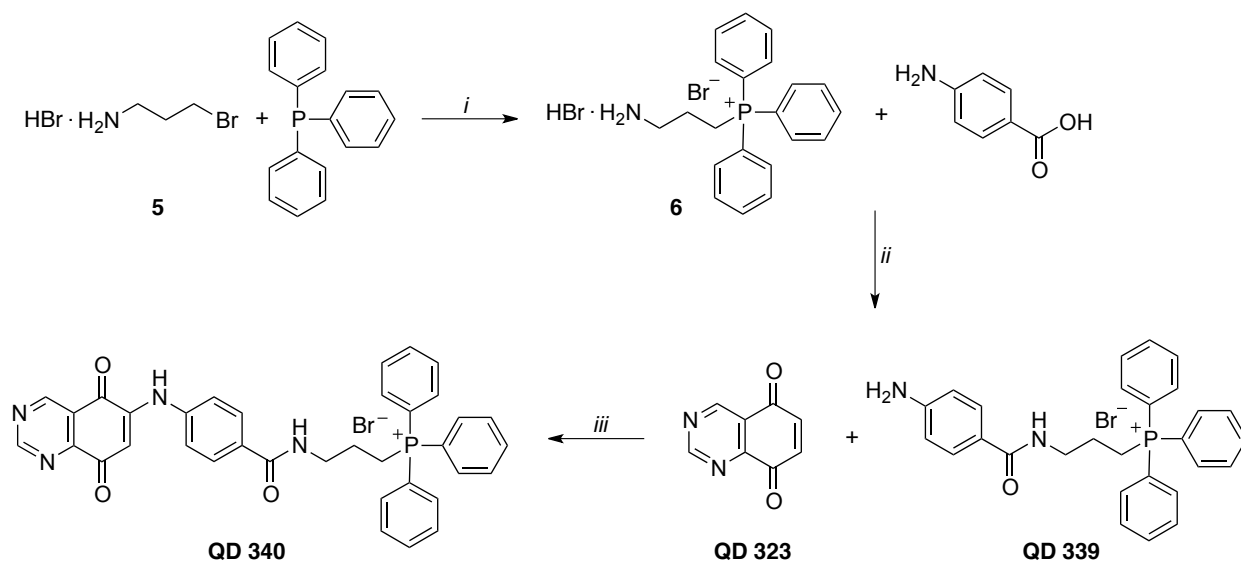
1
2
3 **Scheme 2.**^a Preparation of compounds **QD 324-338, 353-355, 357.**
4
5
6
7



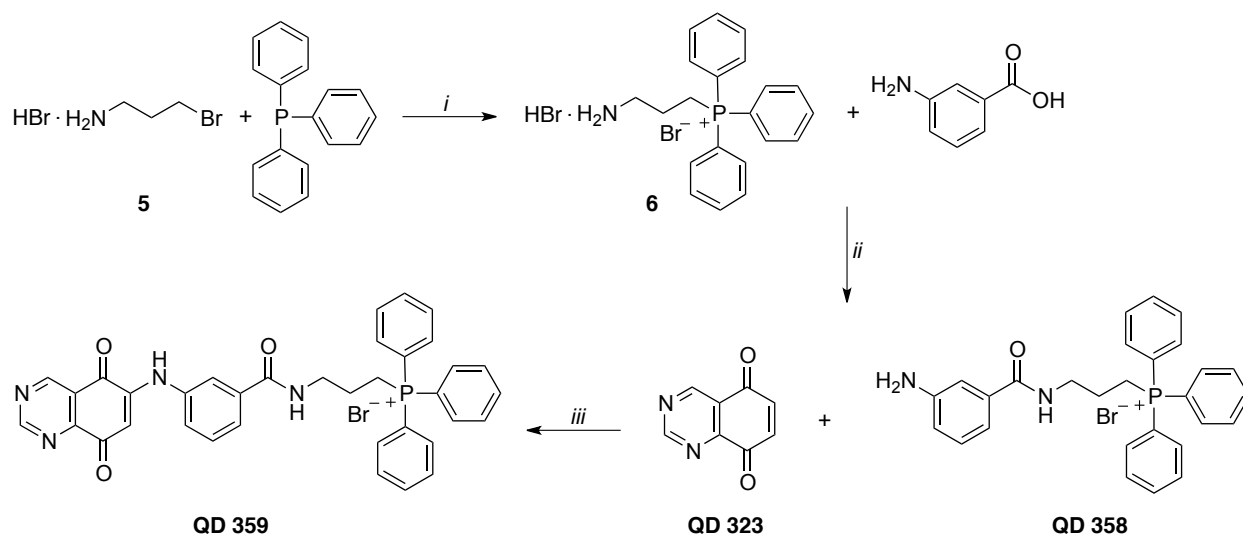
19 ^aReagents and conditions: (i) CeCl₃•7H₂O, abs EtOH, rt, 1-6 h.
20
21
22
23
24
25
26
27
28
29
30
31
32
33
34
35
36
37
38
39
40
41
42
43
44
45
46
47
48
49
50
51
52
53
54
55
56
57
58
59
60

Scheme 3.^a Preparation of QD 356.

^aReagents and conditions: (i) CeCl₃•7H₂O, abs EtOH, rt, 2 h.

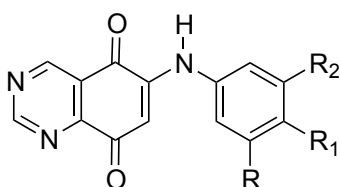
Scheme 4.^a Preparation of QD 339, 340

^aReagents and conditions: (i) MeCN, reflux, 16 h; (ii) 4-aminobenzoic acid, DIPEA, HBTU, DMAP, CH₂Cl₂, rt, 5 h; (iii) CeCl₃·7H₂O, abs EtOH, rt, 2 h.

Scheme 5.^a Preparation of QD 358, 359

^aReagents and conditions: (i) MeCN, reflux, 16 h; (ii) 3-aminobenzoic acid, DIPEA, HBTU, DMAP, CH₂Cl₂, rt, 5 h; (iii) CeCl₃·7H₂O, abs EtOH, rt, 1.5 h.

Table 1. Structure and cytotoxicity of QD compounds in MIA PaCa-2, Panc-1 and BxPC-3 cells by MTT assay. QD compounds are grouped by structure.



QD 232, 324-338, 340, 353-357, 359

| ID | Substitution group | | | IC ₅₀ (μM) ^[1] | | |
|--------------------|---|---|------------------|--------------------------------------|------------|------------|
| | R | R ₁ | R ₂ | MIA PaCa-2 ^[2] | Panc-1 | BxPC-3 |
| 232 | COCH ₃ | H | H | 2.3 ± 0.2 | 0.9 ± 0.2 | 5.2 ± 0.8 |
| 325 | H | Ph | H | 0.9 ± 0.2 | 0.4 ± 0.1 | 0.5 ± 0.1 |
| 335 | H | 4-Et-Ph | H | 2.0 ± 0.1 | 1.2 ± 0.1 | 3.1 ± 0.7 |
| 336 | H | 4-OCH ₃ -Ph | H | 2.1 ± 0.5 | 2.3 ± 0.3 | 3.5 ± 0.5 |
| 337 | H | 4-NH ₂ -Ph | H | 2.5 ± 0.2 | 3.7 ± 0.1 | 3.5 ± 0.6 |
| 334 | H | 4-F-Ph | H | 3.5 ± 1.0 | 3.2 ± 0.8 | 4.4 ± 0.9 |
| 338 | F | 4-CH ₃ -Ph | H | 4.6 ± 1.1 | 4.8 ± 0.1 | 5.0 ± 0.7 |
| 326 | OCH ₃ | OCH ₃ | OCH ₃ | 1.5 ± 0.1 | 0.8 ± 0.1 | 1.6 ± 0.3 |
| 353 | H | H | OCH ₃ | 1.8 ± 0.3 | 0.6 ± 0.1 | 1.8 ± 0.1 |
| 354 | H | OCH ₃ | H | 1.9 ± 0.2 | 0.8 ± 0.2 | 1.7 ± 0.2 |
| 355 | H | OCH ₃ | OCH ₃ | 1.8 ± 0.1 | 0.9 ± 0.3 | 1.5 ± 0.2 |
| 357 | OCH ₃ | H | OCH ₃ | 7.7 ± 2.0 | 7.2 ± 0.8 | 16.3 ± 1.5 |
| 327 | H | OCF ₃ | H | 1.4 ± 0.2 | 0.9 ± 0.1 | 0.9 ± 0.1 |
| 324 | H | O-Ph | H | 3.7 ± 0.7 | 1.8 ± 0.2 | 3.6 ± 0.4 |
| 328 | H | SO ₂ NH ₂ | H | >10 | >10 | >10 |
| 333 | B(OH) ₂ | H | H | >10 | 9.0 ± 1.0 | >10 |
| 331 | H | COOCH ₃ | H | 2.2 ± 0.4 | 1.1 ± 0.4 | 5.8 ± 0.3 |
| 329 | H | CH ₂ OH | H | 3.5 ± 1.3 | 1.0 ± 0.2 | 5.7 ± 0.3 |
| 332 | H | COOCH ₂ CH ₃ | H | 5.5 ± 1.5 | 1.6 ± 0.3 | 5.9 ± 0.1 |
| 330 | H | CONH ₂ | H | 8.0 ± 0.9 | 6.3 ± 0.3 | >10 |
| 323 ^[2] | N/A | N/A | N/A | 9.4 ± 0.9 | 18.0 ± 2.5 | 19.4 ± 1.6 |
| 356 ^[3] | N/A | N/A | N/A | 1.7 ± 0.2 | 1.0 ± 0.1 | 1.4 ± 0.2 |
| 339 ^[4] | N/A | N/A | N/A | >30 | >30 | >30 |
| 358 ^[5] | N/A | N/A | N/A | >30 | >30 | >30 |
| 331 | H | COOCH ₃ | H | 2.2 ± 0.4 | 1.1 ± 0.4 | 5.8 ± 0.3 |
| 340 | H | CONH(CH ₂) ₃ (TPP) ⁺ Br ^{-[5]} | H | 15.3 ± 2.5 | 11.7 ± 1.5 | 21.5 ± 2.3 |
| 232 | COCH ₃ | H | H | 2.3 ± 0.2 | 0.9 ± 0.2 | 5.2 ± 0.8 |
| 359 | CONH(CH ₂) ₃ (TPP) ⁺ Br ^{-[6]} | H | H | 16.3 ± 3.5 | 14.3 ± 1.5 | 21.3 ± 2.5 |

^[1] Data is presented as mean ± SD from three independent experiments.

^[2] Structure of intermediate QD 323 is shown in **Scheme 1**.

^[3] Structure of QD 356 is shown in **Scheme 3**.

^[4] Structure of intermediate QD 339 is shown in **Scheme 4**.

^[5] Structure of intermediate QD 358 is shown in **Scheme 5**.

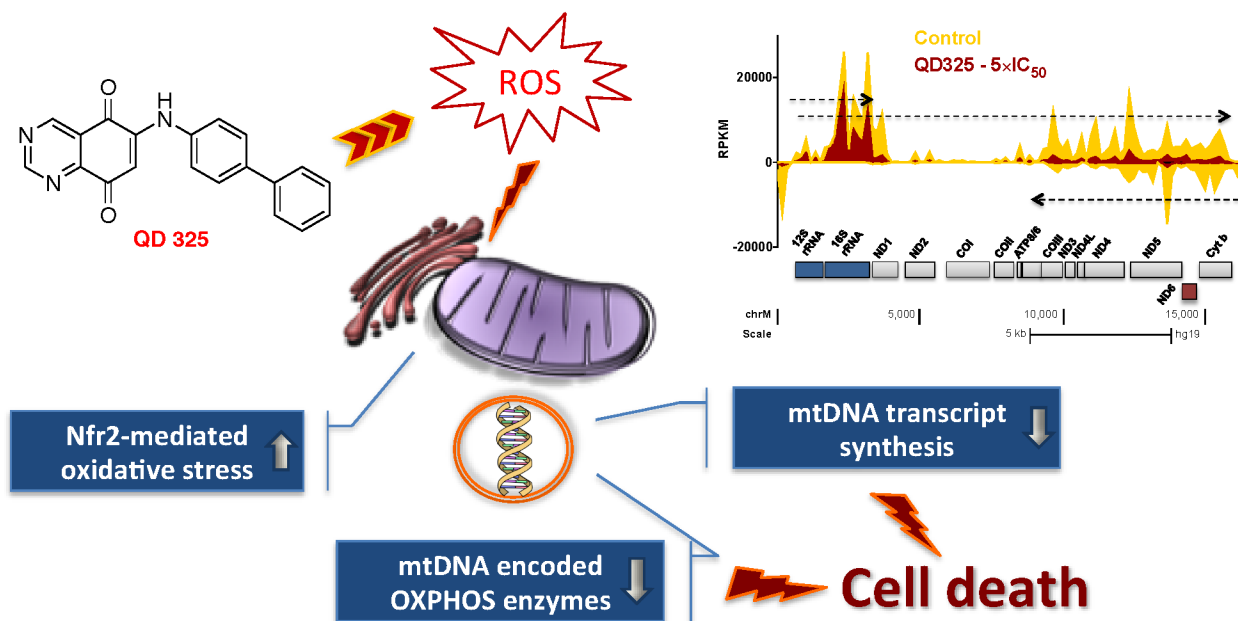
^[6] TPP stands for triphenylphosphonium.

Table 2. Cytotoxicity of QD compounds in gemcitabine resistant MIA PaCa-2 cells and normal pancreatic cells by MTT assay

| ID | IC ₅₀ (μM) ^[1] | | |
|--------------------|--------------------------------------|---------------|-------------|
| | MIA PaCa-2 | MIA PaCa-2-GR | HPDE |
| 232 | 2.3 ± 0.2 | 3.6 ± 0.6 | 4.5 ± 0.6 |
| 325 | 0.9 ± 0.2 | 1.0 ± 0.3 | 2.7 ± 0.3 |
| 326 | 1.5 ± 0.1 | 2.0 ± 0.1 | 3.2 ± 0.4 |
| 340 | 15.3 ± 2.5 | 17.7 ± 1.8 | 18.3 ± 2.1 |
| 359 | 16.3 ± 3.5 | 16.2 ± 1.9 | 24.3 ± 1.2 |
| Gemcitabine | 0.11 ± 0.07 | 3.3 ± 0.6 | 0.14 ± 0.05 |

^[1] Data is presented as mean ± SD from three independent experiments.

TOC Graphics



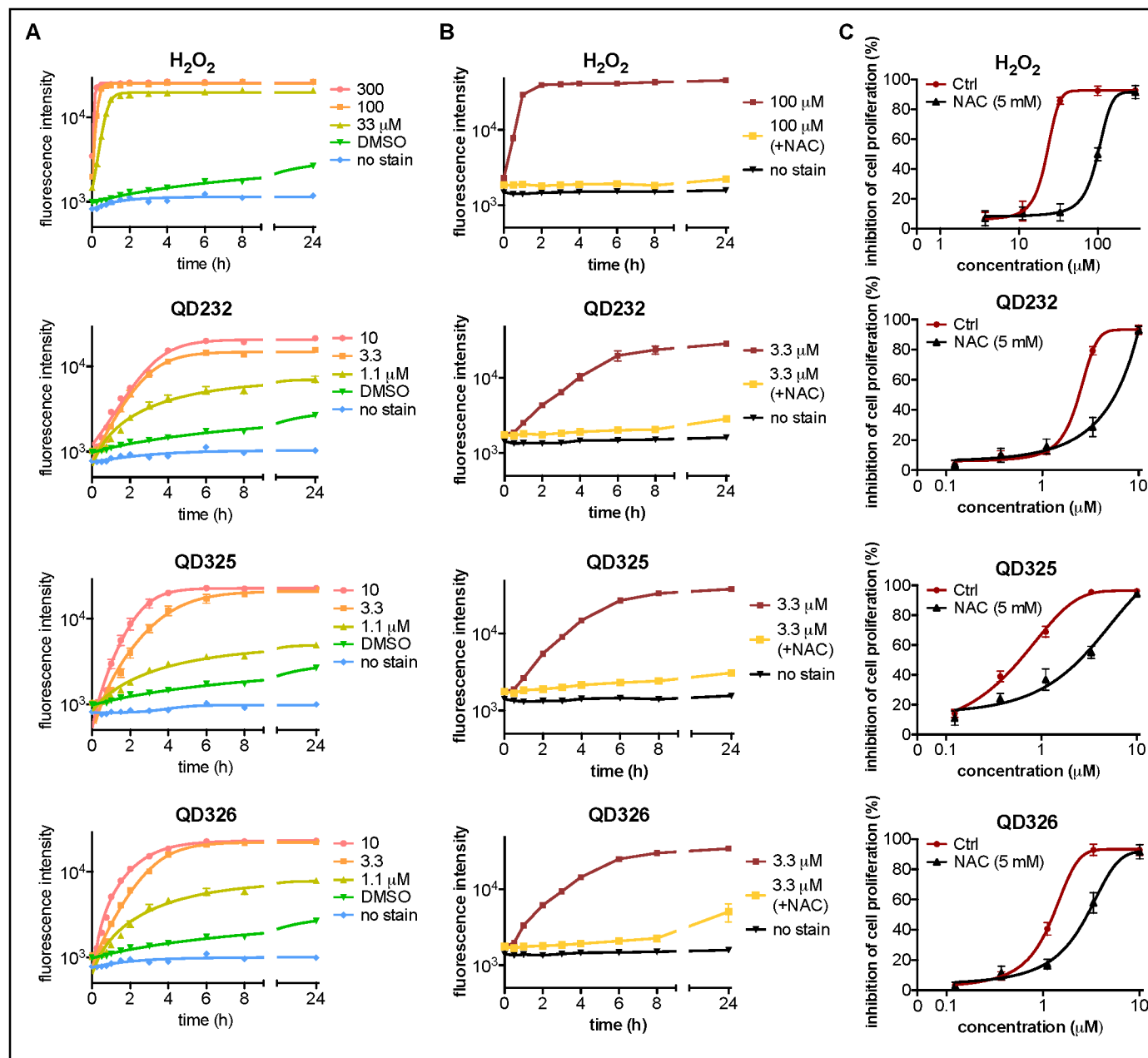


Figure 1

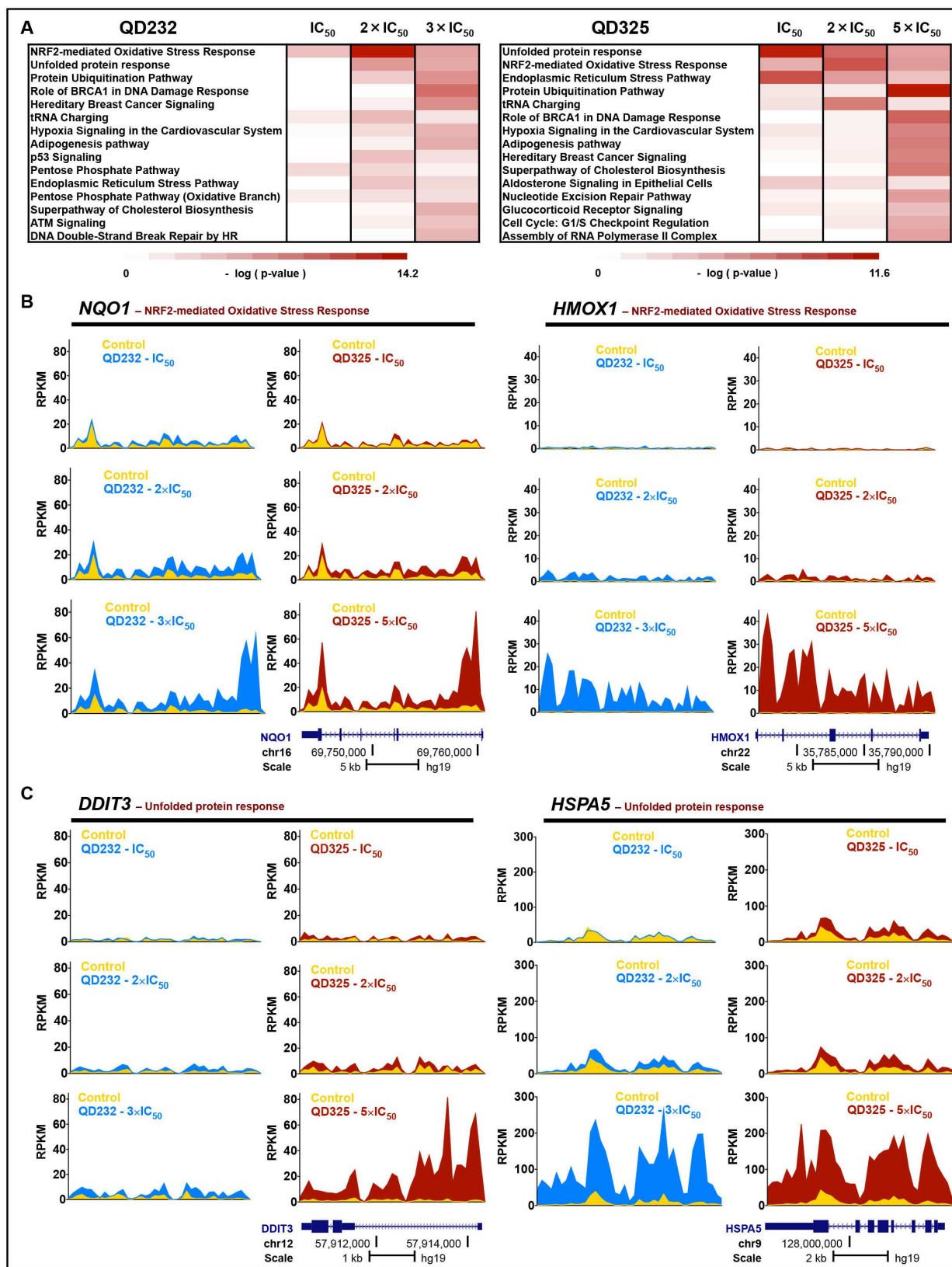


Figure 2

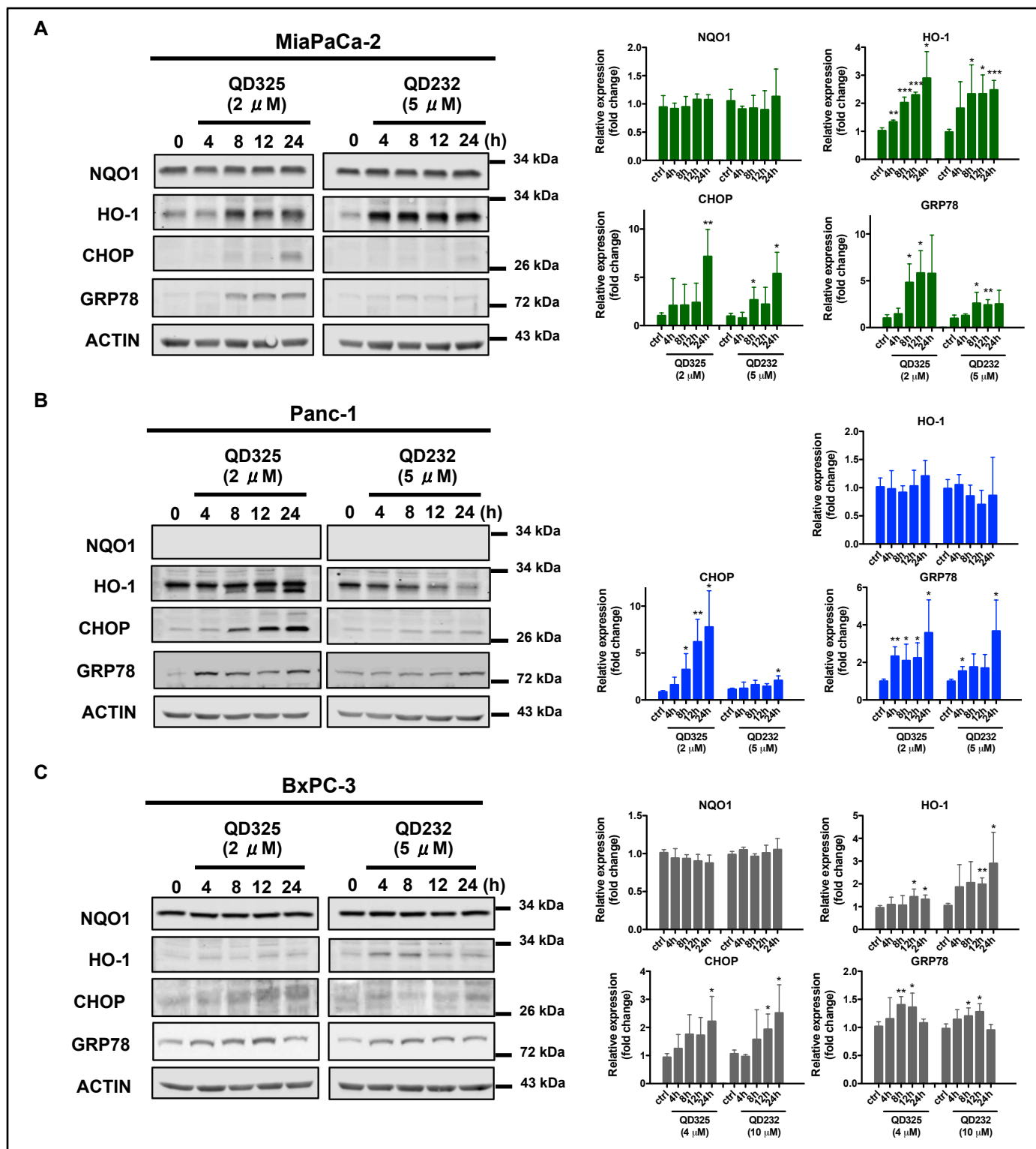


Figure 3

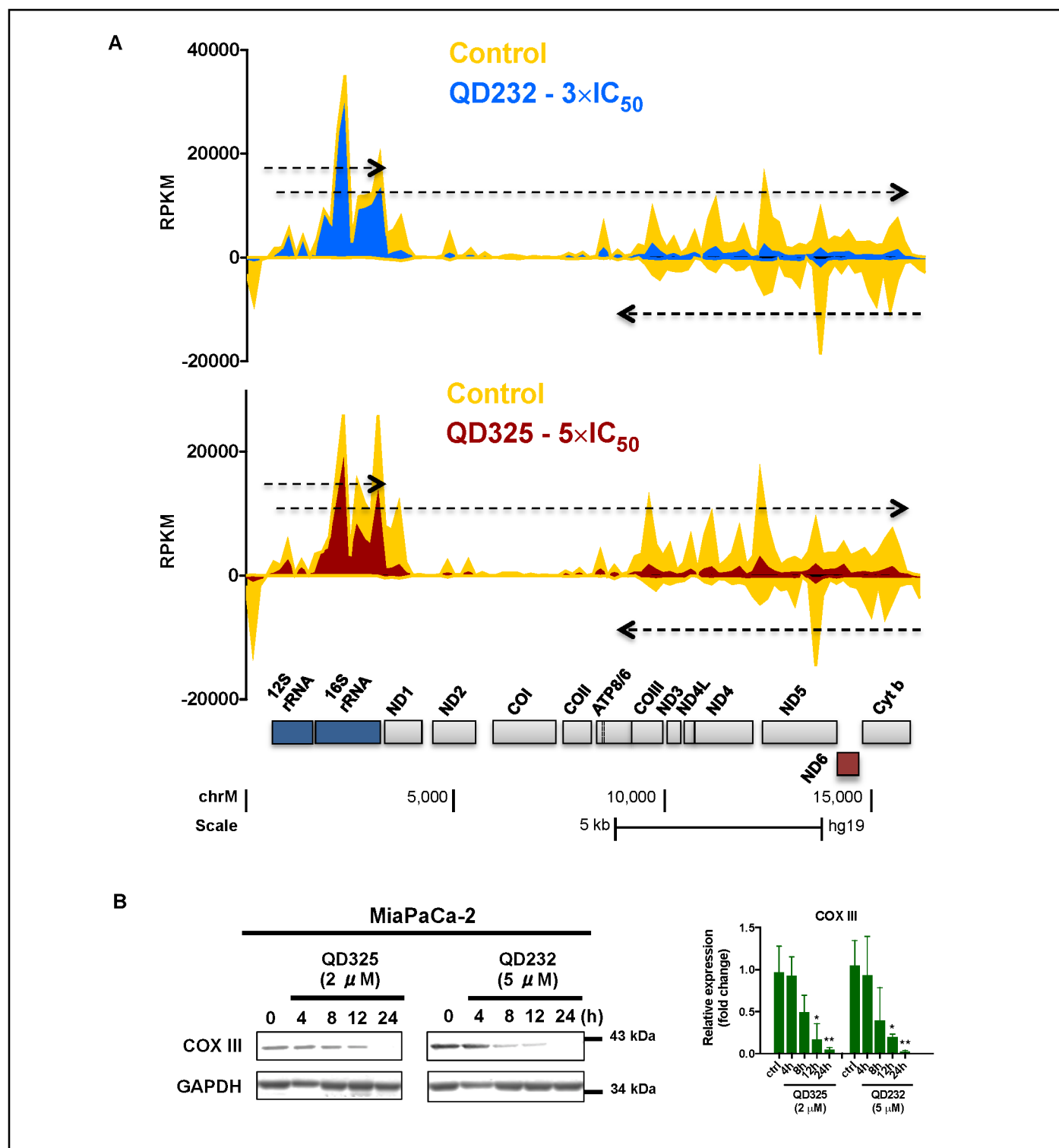
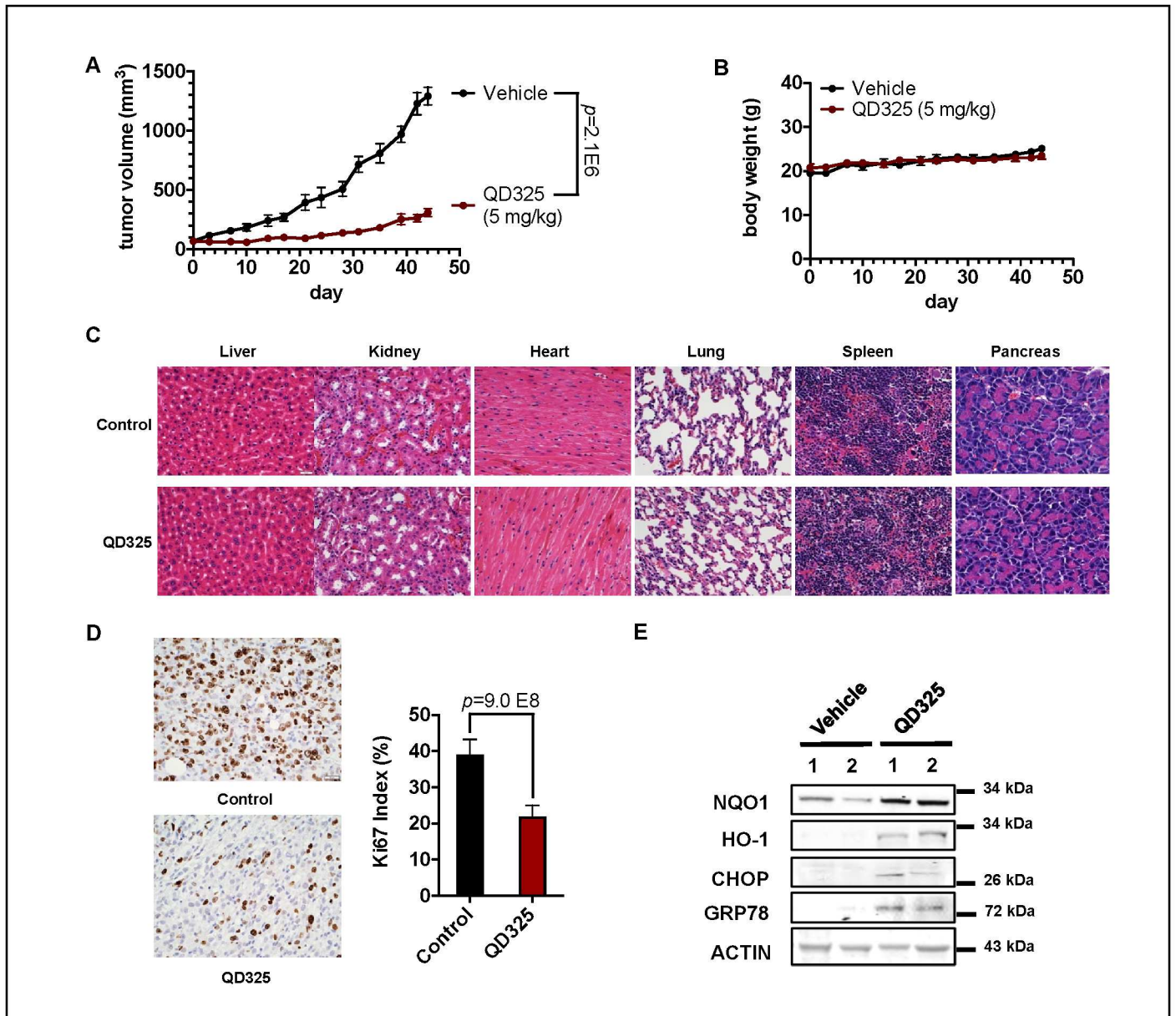


Figure 4

**Figure 5**

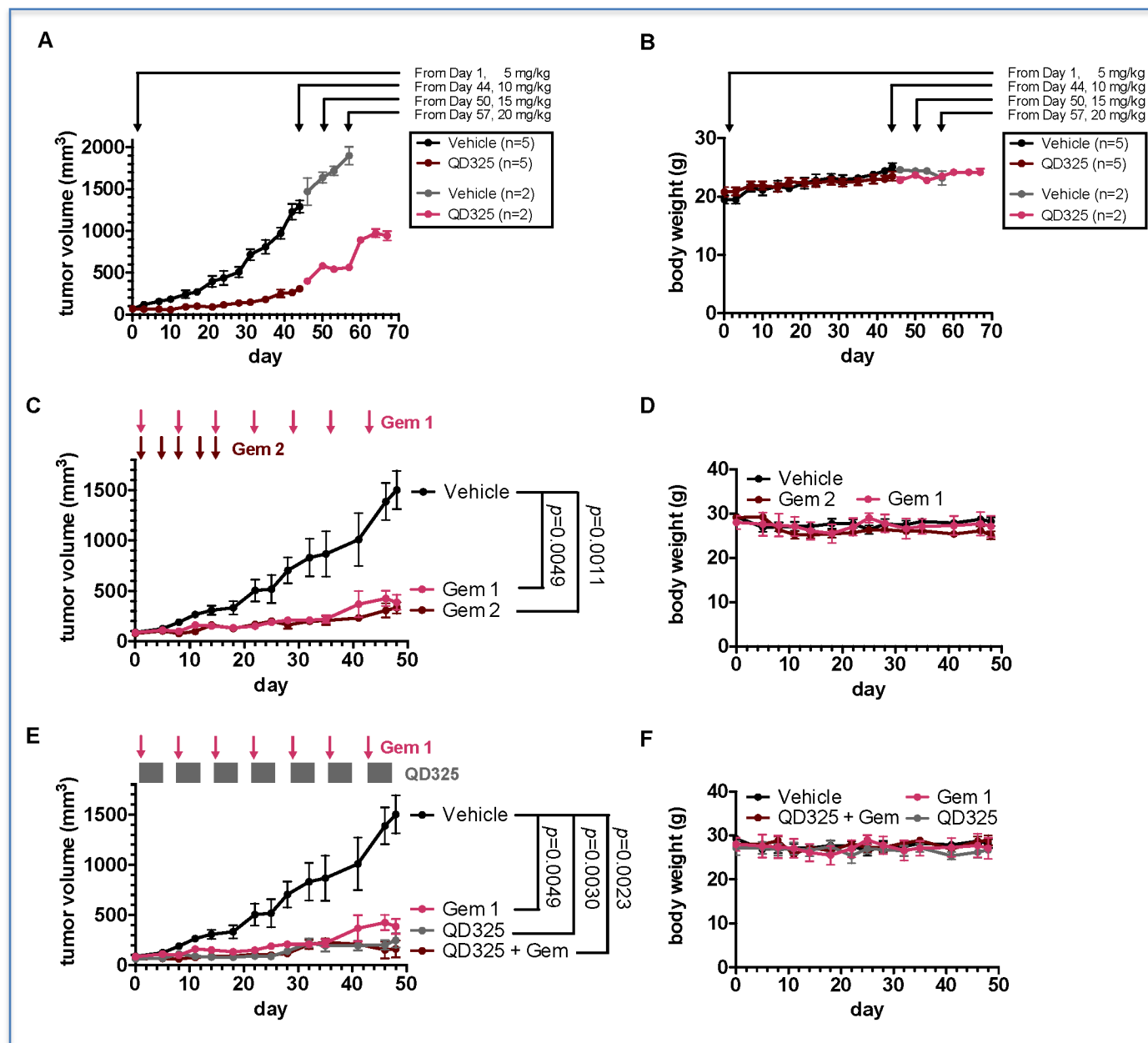


Figure 6